Rho GTPase Signalling Dynamics in Migrating and Non-Migrating Endothelial Cells

Ila Ghoshal

Department of Biology, McGill University, Montreal

June 2022

A thesis submitted to McGill University in partial fulfillment of the requirements of the degree of Master of Science

Table of Contents

List of Figures and Tables i

Abstract ii

Résumé iii

Acknowledgements iv

Contributions of Authors v

List of Abbreviations vi

1 INTRODUCTION 1

2 LITERATURE REVIEW 4

2.1 Cell Migration 4

2.2 Influence of the Cellular Environment on Migration 5

2.3 Front-Rear Cell Polarization 5

2.4 Rho GTPases 7

2.5 Regulation of Rho GTPase Activity 9

2.6 Förster Resonance Energy Transfer 11

2.7 Spatiotemporal Analysis of Rho GTPase Activity in Migrating Cells 13

2.8 Cell-Matrix Adhesions 15

2.9 Cell-Cell Junctions 17

2.10 Extracellular Matrix Micropatterning 18

2.11 Studying Cell Polarity and Migration Using Micropatterns of Extracellular Matrix 20

2.12 Morphometrics 21

3 METHODS 24

3.1 Micropatterning 24

3.2 Cell Culture 25

3.3 Microscopy 26

3.4 Live Cell Imaging of Cells on Micropatterns 27

3.5 Live Cell Imaging of Mosaic Monolayers 27

3.6 FRET 28

3.7 Cell Edge Window Analysis 28

3.8 Rho GTPase Buildup and Decay 29

3.9 Rho GTPase Gradient Analysis 29

3.10 Morphometrics 30

3.11 Computational Determination of Cell Motility Parameters 30
3.12 Spatial Propagation of Rho GTPase activity 30
3.13 Data Visualization 30
4 RESULTS 31
4.1 Using Micropatterns of ECM Proteins for the Study of Cell Motile Behaviour 31
4.2 Pattern Width and Cell Elongation Impact Likelihood of Directed Migration on Micropatterned Lines of Extracellular Matrix 32
4.3 Cells with Periodic Protrusion-Retraction Cycles Have Tightly Regulated Oscillatory Rho GTPase Signalling Dynamics 37
4.4 Rho Signalling Dynamics Depend on Properties of Retraction in Cells Migrating on Lines of Extracellular Matrix 43
4.5 Pattern Area Impacts Cell Motile Behavior on Micropatterned Circles of Extracellular Matrix 46
4.6 Front-Back Gradients of Rho and Rac Activity Have Different Relationships to Net Displacement in Collectively Migrating Cells 48
4.7 Cell Shape Is Not Sufficient to Predict Migratory Phenotype of Collectively Migrating Cells 53
5 DISCUSSION 56
6 CONCLUSION 63
7 REFERENCES 64

List of Figures and Tables

Figure 1. Migrating cells have polarized morphologies. 6
Figure 2. Textbook view of Rho GTPase activity in migrating cells. 8
Figure 3. Regulation of typical Rho GTPase cycling by GEFs, GAP and GDIs. 10
Figure 4. Commonly used micropatterning techniques. 19
Figure 5. Generating micropatterns of ECM proteins 25
Figure 6. FRET probes. 28
Figure 7. Analysis of morphology and motility for cells plated on micropatterned lines. 33
Figure 8. Cells with increased area, length and aspect ratio migrate lesser distances. 34
Figure 9. Cell elongation and cell area contribute to the likelihood of a given cell migrating.... 35
Figure 10. Cells with protrusion-retraction cycles have oscillatory Rho GTPase dynamics. 37
Figure 11. Characterization of Rho GTPase signalling dynamics in cells with periodic protrusion-retraction cycles on micropatterned lines. 41
Figure 12. Rho signalling dynamics depend on properties of retraction in cells migrating on lines of extracellular matrix. 45
Figure 13. Cells plated on micropatterned circles exhibit different types of protrusive activities.. 47
Figure 14. Examples of Rho GTPase signalling in collectively migrating cells. 49
Figure 15. Rho and Rac signalling patterns differ in collectively migrating cells 51
Figure 16. Analysis of morphology and motility for cells plated on micropatterned lines.. 53
Figure 17. Cell shape is not sufficient to predict migratory phenotype of collectively migrating cells 54

Table 1. Antibiotics used for cell culture maintenance. 25
Table 2. Optical Configurations for Imaging. 26

Abstract

Cell migration underlies key biological processes such as wound healing, morphogenesis, and immune response. It is directed by chemical and mechanical cues from the cellular environment, which can induce morphological cell polarization. Rho GTPases are mediators of the cytoskeletal reorganization necessary for establishing and maintaining this polarization. However, their spatiotemporal dynamics during cell migration have not been fully characterized. We aim to gain a greater understanding of the Rho GTPase signalling dynamics that drive autonomous cell migration and to determine how these dynamics are modified in collectively migrating cells. We use micropatterns of extracellular matrix proteins and FRET-based biosensors to investigate the effect of cell shape on cell motile behaviour, as well as the spatiotemporal signalling dynamics of different cell motile behaviours. For this, we compare the signalling dynamics of autonomously migrating and non-migrating cells, as well as signalling in autonomously migrating and collectively migrating cells. Here, we show that larger and longer cells with a more elongated shape are unlikely to migrate along micropatterned lines. We find the steepness of a cell's Rho activity gradient is not related to its net displacement, while there is a relationship between the steepness of the Rac activity gradient and net displacement. We demonstrate that the level of Rho activity in retractions is linked to its duration, however, Rac activity levels do not appear related to protrusion duration. Finally, we find that broadly, the Rho GTPase signalling activities of autonomously and collectively migrating cells are similar, but collectively migrating cells adopt a far narrower range of morphologies compared to cells plated on micropatterned lines.

Résumé

La migration cellulaire contribue à des processus biologiques clés tels que la réparation de plaies, la morphogenèse et la réponse immunitaire. Elle est dirigée par des signaux chimiques et mécaniques provenant de l'environnement cellulaire, qui peuvent induire la polarisation cellulaire. Les petites GTPases de la famille Rho sont médiatrices de la réorganisation du cytosquelette nécessaire pour l'établissement et le maintien de cette polarisation. Pourtant, la dynamique spatiotemporelle de ces protéines n'a pas été complétement caractérisée. Le but de notre étude est d'acquérir une meilleure compréhension de la signalisation des GTPases Rho qui dirigent la migration cellulaire autonome. Nous voulons aussi déterminer comment cette signalisation est modifiée dans les cellules qui migrent de manière collective. Nous avons utilisé des « micro-motifs » composés de protéines de matrice extra-cellulaire et des sondes basées sur le transfert d'énergie par résonance de type Förster (FRET) pour investiguer les effets de la forme sur le comportement motile des cellules, ainsi que la dynamique spatiotemporelle des GTPases Rho impliquée dans de différents comportements motiles observées. Nous comparons la dynamique de signalisation des cellules qui migrent de manière autonome à celle de cellules non-migrantes. Nous comparons aussi la dynamique de signalisation dans les cellules qui migrent de manière autonome à celle de cellules qui migrent de manière collective. Ici, nous montrons que l'aire occupée par une cellule, sa longueur et son dégrée d'élongation influencent son habileté à migrer de manière autonome sur des lignes de matrice extra-cellulaire. Nous trouvons que le déplacement net d'une cellule ne semble pas affecté par le gradient d'activité de Rho, cependant le gradient d'activité de Rac semble lié à celui-ci. Nous démontrons que le niveau d'activité de Rho dans une rétraction dépend de sa durée, mais une relation similaire ne semble pas exister entre le niveau d'activité de Rac dans une protrusion et sa durée. Finalement, nous trouvons qu'en général, la dynamique de signalisation des petites GTPases Rho reste similaire entre les cellules qui migrent de manière autonome et les cellules qui migrent collectivement, mais que les cellules qui migrent collectivement adoptent une gamme de formes restreintes comparée aux cellules sur les lignes de matrice extra-cellulaire.

Acknowledgements

I would like to first thank Dr. Arnold Hayer for his support and his advice on experiments, presentations and writing over the last two years. While starting a Master's project during a pandemic had its challenges, your patience and enthusiasm for science made it a great experience. I would also like to thank my supervisory committee members, Dr. Allen Ehrlicher and Dr. Gary Brouhard for their helpful feedback on my project. I am very grateful for my labmates Baishali Mukherjee, Rodrigo Migueles Ramirez, Qiyao Lin and Nada El Baba. Thank you for your feedback and advice on my research, for commiserating over experimental difficulties and uncooperative code with me, and for all of the laughs in the student office. I would additionally like to thank Rodrigo Migueles Ramirez for reviewing the French translation of my abstract. To my friends, thank you for listening to me talk about my research, for checking in on me and for making sure I was taking breaks when needed. Finally, I would like to thank my parents for their encouragement and reassurance. You have pushed me to do my best, and I am incredibly appreciative of the support you have given me.

Contributions of Authors

I wrote the entirety of this thesis, all of which was revised and edited by Dr. Hayer. I conducted all experimental work for this project, and experiments were planned under the guidance of Dr. Hayer. Cell lines used in this work had been previously established by Dr. Hayer. The FRET and edge velocity analysis code, used in sections 4.3, 4.4 and 4.6, was provided by Dr. Hayer and written in part by Seph Marshall-Burghardt. I made small modifications to this code. The code for calculating the steepness of Rho GTPase gradients of collectively migrating cells used in section 4.6 was written by Dr. Hayer and modified as necessary by myself. I wrote the code used in section 4.4 to calculate the steepness of Rho activity gradients in autonomously migrating cells using code from Baishali Mukherjee. I wrote all other code used in sections 4.2-4.7. I conducted the data analysis featured in sections 4.2-4.7, and prepared the tables (sections 3.2, 3.3) and figures (sections 3.1, 3.6, 4.2-4.7). Dr. Hayer made the diagrams of Rho GTPase probes featured in figure 6 (panels A and B) in section 3.6 and they were included with his permission.

List of Abbreviations

AF	Alexa Fluor
AJ	Adherens junction
AR	Aspect ratio
Arp2/3	Actin-related protein-2/3
Cdc	Cell division cycle
CFP	Cyan fluorescent protein
CV	Coefficient of variation
DMD	Digital micromirror device
DOCK	Dedicator of cytokinesis
DORA	Dimerization optimized reporter for activation
ECB	Extracellular buffer
ECM	Extracellular matrix
EMT	Epithelial-mesenchymal transition
EndMT	Endothelial-mesenchymal transition
FA	Focal adhesions
FACS	Fluorescence-activated cell sorting
FLIM	Fluorescence Lifetime Imaging Microscopy
FMNL2	Formin Like 2
FRET	Forster Resonance Energy Transfer
FSS	Fluid shear stress
GAP	Guanine activating protein
GDI	Guanine dissociation inhibitor

GDP	Guanine diphosphate
GEF	Guanine exchange factor
GPCR	G-protein coupled receptor
GTP	Guanine triphosphate
HT	hTERT
hTERT	Human telomerase reverse transcriptase
HUVEC	Human umbilical vein endothelial cell
LIMK	LIM kinase
LIS	Live imaging solution
mDia	Membrane diaphanous
MLC	Myosin light chain
MLCK	Myosin light chain kinase
MYL	Myosin light chain
PAK	p21-activated kinase
PBS	Phosphate-buffered saline
PCA	Principal component analysis
PDGF	Platelet-derived growth factor
PDMS	Polydimethylsiloxane
PECAM	Platelet endothelial cell adhesion molecule
PEG	Polyethylene glycol
PI3K	Phosphoinositide 3-kinase
PIP3	Phosphatidylinositol (3,4,5)-triphosphate
PKN	Protein kinase N

PLL	Poly-l-lysine
PTM	Post-translational modifications
Rac	Ras-related C3 botulinum toxin substrate
RFP	Red fluorescent protein
STICS	Spatiotemporal image correlation spectroscopy
PIV	Particle image velocimetry
Rho	Ras homologous
ROCK	Rho-associated protein kinase
RTK	Receptor tyrosine kinase
sCMOS	scientific Complementary Metal–Oxide–Semiconductor
TGFβ	Transforming growth factor β
TIRF	Total internal reflection fluorescence
tSNE	t-distributed stochastic neighbor embedding
VAMPIRE	Visually Aided Morpho-Phenotyping Image Recognition
VASP	Vasodilator-stimulated phosphoprotein
VE	Vascular endothelial
VEGF	Vascular endothelial growth factor
WASP	Wiskott-Aldrich syndrome protein
WAVE	WASP-family verprolin-homologous protein
YFP	Yellow fluorescent protein

1 INTRODUCTION

Cell migration plays an important role in key physiological and pathophysiological processes, including wound healing, morphogenesis, immune response, and cancer metastasis (1,2). Autonomously migrating cells integrate chemical and mechanical cues from their environment, and collectively migrating cells additionally receive cues from their neighbours (1,3,4). In response to these cues, cells acquire a polarized morphology, where they form a defined front and rear (4). Cytoskeletal structures, such as actin-rich lamellipodia and filopodia drive membrane protrusions at the cell front, and myosin contractility at the cell rear mediates membrane retractions (5). Underlying this morphological polarization are the polarized activities of Rho GTPases, which transduce signals from the cellular environment to the cytoskeleton and are major mediators of cytoskeletal reorganization (5). The simplified view of Rho GTPase activity in migrating cells posits that cells have front-to-back gradients of Rac and Cdc42 activity, as well as a back-to-front gradient of Rho activity.

Recent studies have painted a far more complex picture of Rho GTPase signalling in cell migration, exploring its precise spatiotemporal regulation by different proteins and post translational modifications (6,7). The use of Förster Resonance Energy Transfer (FRET)-based biosensors to quantify the relative amounts of GTP-bound and GDP-bound Rho GTPases has been a valuable tool for such studies of Rho GTPase activities (8–10). The use of these biosensors, as well as the use of localization-based biosensors, has led to the identification of multiple positive and negative regulatory feedback loops, and the proposed involvement of several excitable signalling networks in cell protrusions and contractions (11–13). Nevertheless, the spatiotemporal signalling dynamics of Rho GTPases required for cell migration remain incompletely understood.

One of the major challenges associated with using FRET-based biosensors to study Rho GTPase signalling in migrating cells is the heterogeneity of cell behaviours on 2D substrates. This heterogeneity can lead to difficulties in comparing the signalling dynamics of cells to each other, or in comparing the activities of different GTPases to each other. To overcome this challenge, we use micropatterns of extracellular matrix (ECM) proteins to control cell shape, ensuring that we can reliably observe behaviours of interest, and to allow us to take parallel measurements of Rho GTPase activity in different cells. In addition, the use of micropatterns allows us to influence the internal organization and polarity of cells (14). In particular, micropatterns can be used to control cytoskeletal architecture and dynamics, as well as the distribution of focal adhesions of cells, thus affecting intracellular signalling pathways (15).

Our overarching goals are to gain a greater understanding of the morphological and Rho GTPase signalling requirements for autonomous cell migration, and to determine how they are modified in collectively migrating cells. To this end, we first seek to understand the morphological requirements for autonomous migration cells by examining the relationship between adhesion surface geometry and cell motility in migrating and non-migrating cells on micropatterned lines. We further aim to quantify the Rho GTPase signalling dynamics of autonomously migrating and non-migrating cells to understand how they differ. We then compare these signalling dynamics to those of cells collectively migrating in 2D in monolayers. Finally, we examine the relationship between cell shape and cell motile behaviour in collectively migrating cells and compare it to the relationship observed in autonomously migrating and non-migrating cells on micropatterned lines.

In section 4.2, we discuss the results of a large-scale comparison of cell motility and morphology for endothelial cells plated on micropatterned lines. We compare the relationships between cell area, cell length and cell elongation and a cell's net displacement, as well as the directional persistence of their migration along micropatterned lines of different widths. We present our findings on Rho GTPase signalling in autonomously migrating and non-migrating Human Umbilical Vein Endothelial Cells (HUVEC) on micropatterned lines of ECM proteins in sections 4.3 and 4.4. We explore the necessity of gradients of Rho activity for autonomous cell migration, the relationship between Rho activity and retraction properties in these cells and the temporal sequence of Rho GTPase signalling in the transitions between protrusions and retractions in non-migrating cells. We further analyze how micropattern area impacts cell motile behaviour on micropatterned circles in section 4.5. In addition, we examine Rho GTPase signalling dynamics in collectively migrating HUVEC in section 4.6. We attempt to gain a greater understanding of the ways in which Rho and Rac signalling differ by comparing the relationship between cell displacement and Rho GTPase activity gradient, and how Rho and Rac activities in retractions and protrusions, respectively, are related to the properties of these edge movement events. Lastly, in section 4.7, we compare the relationship between cell morphology and cell motility in collectively migrating cells.

2 LITERATURE REVIEW

2.1 Cell Migration

Cell migration in multicellular organisms plays a critical role in several normal physiological processes including wound healing, morphogenesis, and immune response (16). As part of these processes *in vivo*, cells sense chemical and mechanical cues from their environment, and will migrate towards or away from them in a directed manner (17). Examples of this include individual neutrophils migrating along gradients of chemokines towards a site of injury (18) and multi-cellular groups of neural crest cells migrating along a stiffness gradient during development (19). Impaired cell migration can lead to a variety of consequences, such as defects in development, immune deficiencies and chronic wounds (2). Additionally, dysregulated cell migration is involved in pathological processes including cancer metastasis and chronic inflammation (2,20). As such, a thorough understanding of this process is vital for the development of effective treatments for many human diseases.

The migration of single cells is often described as a cyclical process. Before this cycle can begin, cells must form a defined front and rear (17). The front of a migrating cell is characterized by actin-rich protrusions, while its rear is typically under high tension (17). This front-rear cell polarization, which occurs in response to external cues, is an important feature of migrating cells (17). Once polarity has been established, a cell will extend a protrusion from its leading edge (5). Next, cell-matrix adhesions will be formed, stabilizing this protrusion, and linking the actin cytoskeleton to the ECM through integrins (5). Through myosin II-mediated contractility, the cell will exert traction forces over its adhesions, resulting in the forward movement of its body (5). Finally, adhesions at the rear of the cell will be disassembled, allowing the cell rear to detach (5).

Depending on cell type and context, cells migrate either autonomously or as part of a group of cells, termed collective cell migration. During collective migration, cells remain connected to each other through cell-cell junctions as they move in the same direction at a similar speed (16,21). This coordinated movement typically allows them to migrate more efficiently than single cells, which can have higher instantaneous velocities but do not migrate as persistently in the same direction (21). Structures such as cadherin fingers, which couple the actin cytoskeletons of neighbouring cells, and cryptic lamellipodia, where cells extend sheet-like protrusions under their neighbours, aid this coordinated movement (22,23).

2.2 Influence of the Cellular Environment on Migration

Migrating cells integrate mechanical, electrical and chemical cues from their environment, which are known to play a role in cell polarization (2,17). During migration *in vivo*, cells encounter a wide range of environments with different topologies, rigidities, degrees of confinement and composed of different ECM proteins (24). Increased substrate rigidity promotes a polarized cytoskeletal organization (17), while confinement in channels with cross-sections similar to cell size can also induce polarization and migration (25). In addition to their role in cell polarization, these differences in environment can lead to cells using different migration modes. Generally, a cancer cell that is exposed to a higher degree of confinement within a 3D matrix will switch from migration using actin polymerization-based protrusions to bleb-driven migration (26). Endothelial cells and some types of epithelial cells are additionally exposed to fluid shear stress (FSS) caused by the friction between blood flow and the cells themselves (27). The amount of FSS to which cells are exposed has been reported to play a role in determining where cells will migrate, with angiogenic sprouting being more likely to occur at sites of low FSS (27).

Cells also polarize in response to the presence of chemoattractants, which include chemokines, growth factors, phospholipid metabolites and formylated peptides (2). Chemoattractants in eukaryotic cells can be divided into two groups, those that bind to G-protein coupled receptors (GPCRs) and those that bind to tyrosine kinase receptors (RTKs) (28). Chemokines belong to the first group, while growth factors belong to the second (28). When the concentration of these diffusible cues is uniform, cells undergo chemokinesis where there is an increase in random migration relative to unstimulated cells (2,28). On the other hand, when there is a gradient of these cues, cells will migrate in a directed manner towards that cue. Gradients of chemoattractant can be established through diffusion of a cue away from a source, by its regulated removal or the gradient can be self-generated (2).

2.3 Front-Rear Cell Polarization

Migrating cells establish a front-rear polarity axis, where the front and rear of these cells are morphologically and biochemically distinct (17,29). Cells typically migrate in the direction of this polarity axis (25). On the scale of a single cell, this polarization results in the reorientation of cytoskeletal structures and organelles (Fig 1). The cell front, or leading edge, is characterized by the presence of plasma membrane protrusions such as lamellipodia, filopodia and blebs (30). In lamellipodia and filopodia, actin polymerization pushes the plasma membrane forward (30). Blebs, however, form when the plasma membrane detaches from the actin cortex, resulting in hydrostatic pressure from cytoplasmic flow pushing the plasma membrane outwards (30).

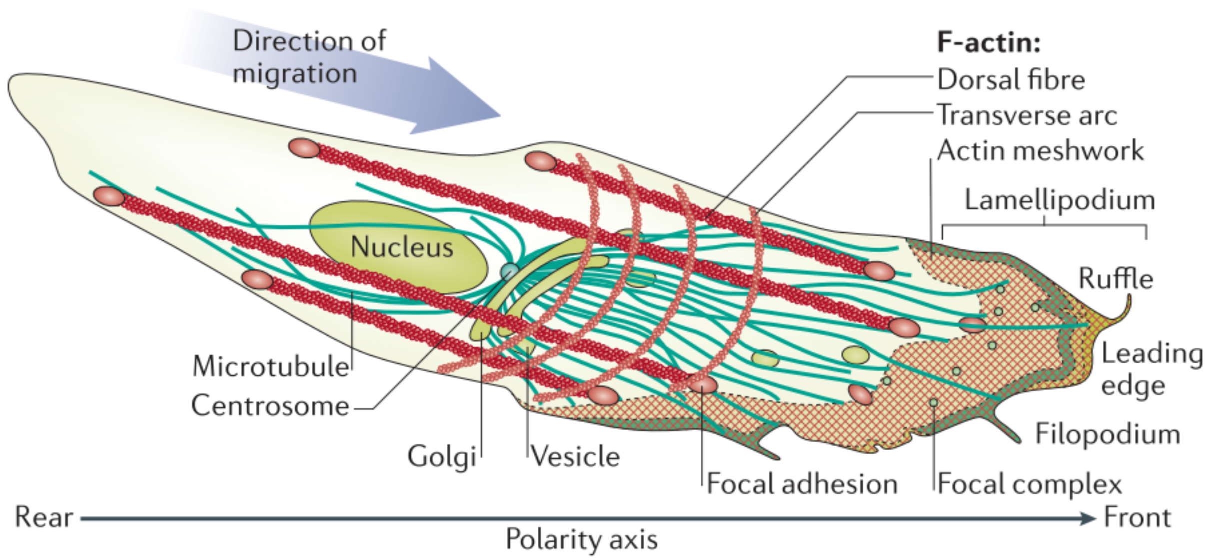

Figure 1. Migrating cells have polarized morphologies. Adapted by permission from Springer Nature: Nature Reviews Molecular Cell Biology, The front and rear of collective cell migration, Mayor and Étienne-Manneville, 2016.

Underlying this morphological polarization are the polarized activities of certain proteins (31). Among these proteins are Rho GTPases, which play a critical role in cell migration as key mediators of cytoskeletal reorganization (31). The polarity complex proteins Par, Crumbs and Scribble are upstream regulators of Rho GTPases which scaffold them to specific membrane domains, thus localizing the activation of Rac and Cdc42 to the leading edge and localizing the activity of Rho to the cell rear (32). The signalling activities of Rho, Rac and Cdc42 and their role in cell migration will be discussed in more detail in the following section.

Within a group of motile cells, polarization can take the form of either the "supracellular" organization of a cluster or the polarization of leader cells at the front of the group (21). Leader and follower cells have different roles within groups of collectively migrating cells (21). Due to their position, leader cells play a critical role in sensing cues from the cellular environment, remodelling the ECM and transmitting directional information to follower cells (21). Follower cells play a role in controlling the speed and direction of migration by communicating with leaders and influencing the polarization of leader cells and of the entire cell cluster (21).

While cells often polarize in response to environmental cues, such cues are not required; fibroblasts, Walker carcinoma cells and fish keratocytes have been reported to polarize spontaneously (33). In spontaneously polarizing fish keratocytes, the cell rear and the perinuclear region were found to exhibit the first signs of polarization, with myosin-mediated contraction and increased F-actin retrograde flow triggering motility initiation, while changes in actin flow at the cell front occurred during later stages of this process (33). Once cells have successfully polarized, branched actin networks can be found at the front with stress fibers running along the length of the cell (21). The activity of cytoskeletal regulators PI3K and PIP3 is polarized in migrating cells, where they are mainly present at the leading edge (25). Downstream regulators such as Arp2/3, as well as the WAVE and WASP complexes are located at the cell front (25). Finally, the organization of adhesions is polarized in migrating cells, with a larger number of nascent adhesions present at the cell front and fewer, more mature adhesions present at the cell rear (34).

2.4 Rho GTPases

Rho GTPase activities are central to all modes of cell migration due to their importance in establishing and maintaining various required structures, such as lamellipodia and filopodia. Rho GTPases are also involved in processes including vesicle trafficking, cytokinesis and endocytosis (35). There are 20 Rho GTPases in humans, the most well-studied of which are RhoA, Rac1 and Cdc42 (36). Typical Rho GTPases cycle between an active, GTP-bound state, in which they are membrane-associated, and an inactive, GDP-bound state (36). Rho GTPases in the GDP-bound state can be sequestered in the cytosol by guanine dissociation inhibitors (GDIs) and thus prevented from localizing to the cell's plasma membrane or being activated by GEFs (37). Rho

GTPases are activated by guanine nucleotide exchange factors (GEFs) and inactivated by GTPase activating proteins (GAPs) (36).

The activities of the three canonical Rho GTPases, Rho, Rac and Cdc42, underlie the front-rear polarization of cytoskeletal structures in migrating cells (31). These signal transducers regulate pathways that link plasma membrane receptors to the actin cytoskeleton, and are also known to regulate microtubule dynamics (35). In the textbook view, Rac and Cdc42 activity are elevated at the front of migrating cells, and the activity of these proteins is associated with the formation of protrusions such as lamellipodia and filopodia at the leading edge (Fig 2) (21). On the other hand, Rho activity is elevated at the cell rear, as it is associated with the myosin-mediated contractility necessary for the retraction of the trailing edge (21).

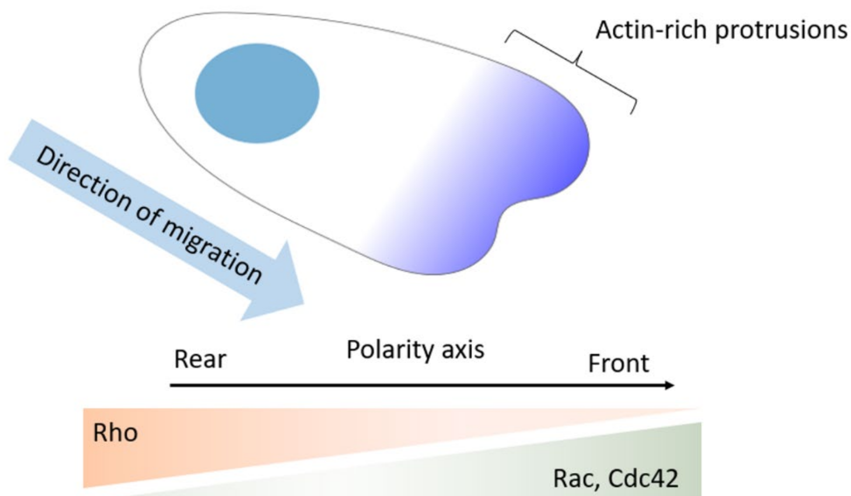

Figure 2. Textbook view of Rho GTPase activity in migrating cells.

To establish and maintain protrusions in migrating cells, Rac and Cdc42 act through WAVE and WASP, respectively, to activate the Arp2/3 complex, which mediates actin polymerization in the lamellipodium by nucleating new branched actin filaments (5). They also act through p21 activating kinase (PAK) and LIM kinase (LIMK) to inactivate the actin-severing protein cofilin through phosphorylation (34). As such, polymerized actin can accumulate at the leading edge (38). Cdc42 additionally acts through a formin, mammalian diaphanous (mDia) 2, and formin-like protein 2 (FMNL2) to induce filopodia (30,39).

The retraction of the cell rear relies on actomyosin contractility, which requires myosin II activation through phosphorylation (5). Rho activity, through Rho-associated protein kinase

(ROCK), results in myosin light chain (MLC) phosphorylation both directly and through the inhibition of myosin light chain phosphatase (5). Myosin light chain kinase (MLCK) also positively regulates MLC phosphorylation (5). In addition, Rho/ROCK signalling has been linked to bleb-driven migration, for which actomyosin contractility is also important (36). Additionally, Rho/ROCK activity has been implicated in filopodium formation, given that Rho/ROCK signalling stimulates fascin binding to actin filaments and that RhoA is a regulator of mDia1 (36).

2.5 Regulation of Rho GTPase Activity

Efficient cell migration requires the coordination of multiple processes, including cell adhesion, actin-driven membrane protrusion and myosin-mediated rear retraction. Active Rho GTPases can interact with a variety of different effector proteins including kinases, actin regulators and cytoskeletal adaptor proteins, resulting in a range of possible cellular responses depending on the downstream targets activated (37). The activity of Rho GTPases, which are involved in many of the processes required for cell migration, must therefore be precisely regulated in space and time. Further, aberrant Rho GTPase signalling has been implicated in cancer and inflammatory diseases (40,41).

Rho GTPases can broadly be divided into two groups: typical Rho GTPases, which cycle between GTP- and GDP-bound states, and atypical Rho GTPases, which are constitutively GTP-bound (37). Typical Rho GTPase activity is regulated at the level of GTP cycling by activating GEFs, which catalyse nucleotide exchange, and inactivating GAPs, which increase the speed of GTP hydrolysis (Fig 3) (42). The human genome encodes 80 Rho GEFs and 66 Rho GAPs, which are often able to regulate the activity of more than one Rho GTPase (13,43). The subcellular localization of Rho GEFs and Rho GAPs affects the downstream effectors with which a given Rho GTPase will interact (37). In mapping the subcellular distribution of Rho GEFs and GAPs, Müller et al. found that over half of them localized to one or more distinct cellular structures at steady state, including focal adhesions, pointing to their important role in spatially controlling Rho GTPase activity (13). Rho GEFs and Rho GAPs also form complexes with effector proteins, as well as cytoskeletal and focal adhesion components, amongst others (6). The complex formed determines which cell behaviours will be impacted and in what fashion

(6). It can additionally impact Rho GTPase localization, depending on which membrane interaction domains are a part of their structure (6).

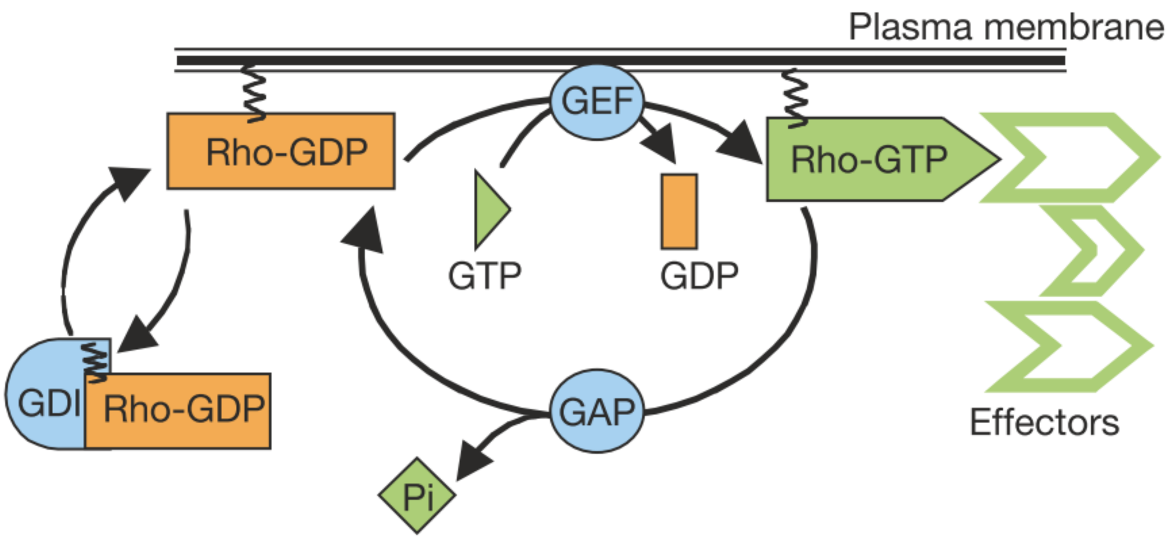

Figure 3. Regulation of typical Rho GTPase cycling by GEFs, GAP and GDIs. Reproduced by permission from Springer Nature: Nature, Rho GTPases in cell biology, Étienne-Manneville and Hall, 2002.

The cycle of Rho GTPase activation and inactivation often involves their association and dissociation from the plasma membrane, where GTP-bound Rho GTPases activate their effectors. Rho GDIs inhibit the dissociation of GDP from Rho GTPases, thus maintaining an inactive pool in the cytosol through sequestration (Fig 3) (44). They can also prevent Rho GEFs from interacting with Rho GTPases, and prevent Rho GTPases from interacting with their effectors (44). GTPases can additionally be extracted from the plasma membrane by GDIs (45). Given that only 3 conventional GDIs exist, competition for binding them to avoid degradation may allow modifications in the binding affinity of one Rho protein to modulate the release, stability or activation of others (45,46).

Crosstalk between Rho GTPases also occurs through the activity of Rho GEFs and Rho GAPs (45). For example, this is known to be the case for RhoA and Rac1 (45). Here, RhoA inhibits Rac1 through ROCK and FilGAP, a Rac GAP (45). ROCK further displaces the Rac GEFs β-Pix and DOCK180 from focal adhesions (45). On the other hand, Rac1 activates p190RhoGEF and acts through PAK to regulate the activity of multiple other Rho GEFs (45).

Rho GTPase crosstalk also occurs when they share common effectors or molecular targets, such as MLC phosphatase and cofilin which are downstream effectors of multiple Rho GTPases (45).

Rho GTPase activities can also be regulated by post-translational modifications (PTMs), miRNAs and at the level of gene expression by transcription factors such as those activated by TGFβ (37,47,48). PTMs that can regulate GTPase activities include lipid modification, phosphorylation and ubiquitination (37). Lipid modifications, such as prenylation and palmitoylation, mediate Rho GTPase association with membranes and localize Rho GTPases to specific membrane compartments, thus directly affecting which GEFs they interact with (37). Phosphorylation of residues within the GTPase domain can affect GTP cycling, and phosphorylation can additionally affect interactions with downstream effectors (37). When phosphorylation occurs near lipid modifications, it can also alter GTPase localization (37). Finally, ubiquitination targets GTPases for degradation, thus controlling their turnover (37). The activity of Rho GEFs, Rho GAPs and Rho GDIs are also regulated by PTMs (37).

2.6 Förster Resonance Energy Transfer

A large body of the research on Rho GTPase signalling in cell migration has been done using tools, such as biochemical pull-down assays, that are not able to accurately capture the spatiotemporal dynamics of Rho GTPase activity within live cells (10). Using FRET-based activity reporters and live-cell microscopy, the activation state of Rho GTPases can be quantified across the cell. The added spatiotemporal resolution provided by FRET probes for Rho GTPase activities has allowed the discovery of signalling activities outside the current dogma. For example, in addition to its activity at the rear of migrating cells, Rho activity has been found to contribute to stabilizing microtubules at the leading edge (10). Given that these tools were developed in the early 2000s, many questions on the signalling networks that control cell migration remain to be answered.

FRET occurs between a donor and an acceptor fluorophore when the two are within 1-10 nm of each other, and the dipoles are in the correct relative orientation (49,50). The emission spectrum of the donor fluorophore must also match the excitation spectrum of the acceptor (51). When the donor fluorophore is in an excited state, it can transfer this excitation energy in a non-radiative manner through long range dipole-dipole interactions (52). This results in a quenching of donor fluorescence and a reduced fluorescence lifetime, as well as an increase in acceptor fluorescence emission (52). As such, the use of FRET-based biosensors is a far more sensitive method for detecting protein-protein interactions than simply looking at the co-localization of two fluorescently tagged proteins.

A number of different FRET probe designs to measure Rho GTPase activity exist, including bimolecular and unimolecular designs. These designs consist of a pair of fluorescent proteins, typically CFP and YFP, conjugated to a Rho GTPase and a Rho GTPase effector protein domain, which are brought closer together upon Rho GTPase activation, thus increasing FRET between the fluorescent proteins (53). For bimolecular probes, the donor and acceptor fluorophores are bound to separate proteins. A change in FRET efficiency occurs if the proteins to which the donor and acceptor fluorophores are fused are in close proximity (10). On the other hand, for unimolecular probes, the donor and acceptor fluorophores are part of a single chain (10). These biosensors detect activation state through the conformational change induced by GTPase cycling, which will bring the donor and acceptor fluorophores closer together or further apart (10). A major advantage of unimolecular probes is that the distribution of donor and acceptor fluorophores is identical within a given cell, thus eliminating the need for corrections addressing the uneven subcellular distribution of the proteins comprising a bimolecular probe (10).

Three commonly used methods for measuring FRET efficiency are ratio-metric FRET, Fluorescence Lifetime Imaging (FLIM), and Acceptor Photobleaching. For ratio-metric FRET, images are taken in the donor and FRET channels, and the ratio of their intensities is computed (52). For Acceptor Photobleaching, FRET efficiency is calculated by measuring the decrease in donor intensity before and after photobleaching of the acceptor (52). A major disadvantage of this technique for studying cell migration is that it can only be performed once (52), and is as such not suitable for determining protein dynamics over the course of a timelapse imaging. Finally, FLIM measures the lifetime of the donor fluorophore. This can be used to determine FRET efficiency as donor fluorescence is quenched when FRET occurs, and the amount of quenching can be measured using the fluorescence decay time of the donor (52). However, the image acquisition time for FLIM is on the order of minutes, which can be an obstacle to implementing this technique to look at faster processes in migration (52).

Localization-based or relocation probes are an alternative to FRET-based biosensors. These probes, which consist of a fluorescent protein-conjugated Rho GTPase effector domain, visualize endogenous Rho-GTP as they are recruited to wherever the GTPase is active. FRET-based biosensors, on the other hand, report on the balance of endogenous GEF and GAP activity (54). Multiple localization-based probes for Rho have currently been published, including an anillin-based based probe and a rhotekin G protein binding domain-based probe (54). While the ability to measure endogenous Rho GTPase activity is an important advantage of these probes, associated drawbacks include their lower specificity compared to FRET-based sensors, the required corrections for intensity changes due to changes in morphology, that the use of a TIRF or confocal is recommended, and that visualizing endogenous Rho GTPase activity may interfere with the biological activity of Rho GTPases (54).

2.7 Spatiotemporal Analysis of Rho GTPase Activity in Migrating Cells

Studies using FRET-based biosensors to determine Rho GTPase activity in migrating cells have discovered the importance of environmental stimuli in determining their spatiotemporal activity patterns. Randomly migrating fibroblasts and persistently migrating PDGF-stimulated fibroblasts were found to have distinct patterns of RhoA activity (55). In PDGF-stimulated cells, RhoA activity is restricted to a narrow strip at the edge of the lamellipodium, whereas in randomly migrating cells, there is a broader activity zone of RhoA at the front of the cell. In both cases, RhoA activity is elevated at the cell's trailing edge (55). In addition, for fibroblasts undergoing cell-cell collisions, Rac1 activity patterns were found to be different in protrusions that touched other cells compared to contact-free protrusions (55).

Taking advantage of the spatiotemporal resolution offered by FRET probes, several studies have employed the methodology of "cell edge window analysis" to perform quantitative analysis of Rho GTPase signalling dynamics. For this, the cell edge was parameterized into a given number of evenly spaced windows, going a certain depth into the cell from the edge, and Rho GTPase activity levels were calculated at multiple time points (9). These signalling activities could then be compared to edge velocity during protrusions and retractions of the cell edge, as well as to the activities of other Rho GTPases by using the start of protrusion or retraction as a reference point (9,56). Recently, FRET probes for Rho GEF activities have been used in cells also expressing redshifted Rho GTPase probes (57). Using the same methodology as above and applying correlation analysis, Marston et al. were able to determine to what extent a specific GEF contributed to the activity of a given GTPase (57).

Using this methodology, Machacek et al. studied the coordination of Rho GTPase signalling during cell edge protrusion in mouse embryonic fibroblasts (9). They found RhoA to be active during edge advancement, while Rac and Cdc42 activity followed with a delay (9). Analysis of the spatial organization of Rho GTPase activity showed RhoA activity to be confined to a 2 μm band at the leading edge, whereas Rac and Cdc42 activity were observed 1.8 μm from the leading edge (9). Overall, their findings suggested that cell morphology and Rho GTPase signalling were tightly coupled in space and time (9). A study of Rho GTPase signalling dynamics in fibroblasts using similar methodology was conducted by Martin et al (56). They found that during PDGF-stimulated cell protrusion, Rac and Cdc42 activity were elevated. Cdc42 activity remained high during both stalling and retractions, while Rac activity remained high during stalling but was reduced in retraction (56). RhoA activity was reduced during protrusion but was increased during stalling and retraction. In Y-27632 treated cells, RhoA signalling dynamics were altered and high RhoA activity was observed during the entire cycle (56). The signalling dynamics of Rac and Cdc42, however, remained similar (56).

Yang et al. used FRET-based biosensors and computational analysis of spatiotemporal Rho GTPase signalling dynamics to study chemotaxis in neutrophil-like cells. Cdc42 and Rac activities were shown to be increased at the front of cells, while RhoA activity was lower at the cell front and higher at the cell rear in chemotaxing cells (8). These cells had steep gradients of Cdc42 and RhoA activity, and shallower gradients of Rac and Ras activity (8). By temporally cross-correlating GTPase activity with the angular direction of migration, Cdc42 and RhoA activity were found to precede cell turning, and evidence showed that Cdc42 antagonized RhoA, making it the primary GTPase steering chemotaxis (8). Unlike Machacek and Martin, the authors did not report elevated RhoA activity in protrusions. Finally, using latrunculin A and "cell edge window analysis", Cdc42 activity was found be locally pulsatile in the absence of actin polymerization, suggesting that Cdc42 is part of an excitable signalling network and fulfilling a requirement of models of chemotactic steering (8).

In addition to chemotactic steering, excitable signalling networks have been proposed to govern cell protrusion and contraction (11). Graessl et al. observed subcellular pulses and propagating waves of Rho activity coupled to subcellular actomyosin contraction and myosin II localization (12). They found that an activator-inhibitor network involving faster self-amplification of Rho by GEF-H1 and slower Rho inhibition by Rho GAP Myo9b were responsible for the spontaneous emergence of pulses and propagating waves of Rho activity (12).

Models of periodic propagating waves of Rho GTPase activity have suggested that they play an important role in coordinating the leading and trailing cell edges during breast cancer cell migration (58). Protrusion-retraction cycles at the front of migrating cells are accompanied by oscillatory RhoA and Rac1 activities, which travel down the length of the cell to its rear, due to diffusion fluxes (58). Rac1 traveling towards the rear of the cell might serve to destabilize focal adhesions there, while RhoA traveling towards the front of the cell could allow focal adhesions to form and allow stress fibers to generate contractile forces needed to pull the rear forward (58). Interfering with this signalling network by inhibiting ROCK activity has been demonstrated to result in multipolar cells, both in simulations and in experiments using ROCK inhibitor (58).

2.8 Cell-Matrix Adhesions

Cell-matrix adhesions are sites where cells engage in physical contact with their environment, as well as important signalling hubs (59). In migrating cells, cell-matrix adhesions form at the leading edge and remain in place as the cell body moves over them. As they mature, they increase in size before disassembling at the cell rear (59). Once nascent adhesions have recruited a sufficient number of transmembrane proteins and cytoskeletal adaptors, they are referred to as focal adhesions (FAs) (59). Using super-resolution microscopy, the Waterman group showed that FAs have a highly organized, stratified structure, made up of three functional layers: an integrin signalling layer, a force transduction layer and an actin regulatory layer (60). Integrins are heterodimeric transmembrane proteins that make up the base of the FA, and they possess an extracellular domain that binds ECM ligands (60). The integrin signalling layer contains the intracellular domain of integrin, focal adhesion kinase and paxillin (60). Talin and vinculin make up the force transduction layer, where talin links integrins to the actin cytoskeleton and vinculin reinforces these linkages (60). Finally, the actin regulatory layer is made up of VASP, zyxin and actin filament termini where VASP and zyxin might be involved in strengthening focal adhesions (60). α-actinin appears along stress fibers, cross-linking them, and aiding in the formation of actin bundles (60).

Actin linkage is essential for FAs, and cells lacking talin 1 and 2, which link integrins to the actin cytoskeleton, are unable to form FAs (61). Further, many of the critical steps for FA assembly depend on or can be promoted by the application of force by the actin cytoskeleton (61). There also exists crosstalk between the actin cytoskeleton and FAs, as the interactions between these adhesions and the cytoskeleton are bidirectional (61). Forces generated by the actomyosin cytoskeleton can affect mechanosensitive proteins that make up the adhesion, such as talin and vinculin (61). If proteins that play a role in integrin signalling are stimulated, they can activate Rho GTPases, which in turn can promote actin polymerization or actomyosin contractility (61).

FAs play an important role in sensing the cell's mechanical environment, since, as previously discussed, substrate stiffness is an important environmental cue for migrating cells (59). Additionally, cells exert mechanical forces on their substrate through their FAs (59). In response to force-induced stretching, both talin and vinculin undergo conformational changes (59). Talin is activated by integrin binding to its rod domain, and when subjected to actomyosin forces, conformational changes in talin expose vinculin binding sites (59). Vinculin is recruited to adhesions by talin and is activated once it binds actin, which induces a conformational change in vinculin, allowing it to recruit a multitude of other proteins, thereby promoting FA growth (59). Further, the recruitment of talin and vinculin to adhesions has been shown to correlate with the mechanical force applied to FAs, with vinculin recruitment occurring in a force dependent manner (59). Certain integrins are also involved in rigidity sensing and are recruited to reinforce adhesions under high tension (59).

Cells transmit traction forces which are required for movement through their cell-matrix adhesions. These forces are generated by the coupling of actin retrograde flow to FAs, which generate pulling forces (59). Stronger mechanical forces are applied to more mature adhesions, however newer adhesions at the cell front are under higher tension than those at the cell rear (59). Integrins form "catch-bonds", where a certain amount of mechanical force increases the strength of the bond, but once a threshold of force applied is crossed, the bond begins to weaken (62). A similar biphasic response exists between the short-term strength of cell-matrix adhesions and the speed of migrating cells, as they need to maintain a balance between applying an adequate amount of force at the cell front and being able to dissociate at the rear (63). Cells migrate fastest at intermediate ECM ligand concentrations, with intermediate integrin expression levels, and intermediate ligand-binding affinity states (63).

2.9 Cell-Cell Junctions

Cell-cell adhesions link cells to their neighbours and are necessary for the organization of cells into tissues. They are further required for the coordinated movement of collectively migrating cells (21). Several types of cell-cell adhesions exist and play a role in maintaining tissue cohesion, including tight junctions, gap junctions and desmosomes (64). They are formed by different types of cell-cell adhesion receptors, which in turn are linked to distinct cytoskeletal structures (64). Adherens junctions (AJs) are the cell-cell junction type with the best established role in force transmission between cells, and the primary site of their mechanical coupling (64,65). These junctions, along with others, link the cytoskeletons of neighbouring cells. They are composed of cadherins, catenins and vinculin (59). Cadherins are transmembrane proteins which interact homotypically with the cadherins of neighbouring cells (59). Several types of cadherins exist and their expression is cell type dependent, with VE-cadherin being characteristic of endothelial cells. Within the cell, cadherins form a complex with catenins (α, β and p120) (59). β-catenin and p120 catenin bind the cytoplasmic tail of cadherins, and α-catenin binds β-catenin (59,66). When α-catenin is stretched, it undergoes conformational changes and can bind F-actin directly or through vinculin (59). Cell-cell and focal adhesions are both linked to the actin cytoskeleton, and studies suggest that increasing the strength of either cell-matrix adhesions or cell-cell adhesions leads to a decrease in the strength of the other. As such, these forces are balanced in monolayers, where increasing cell-substrate forces results in less coordinated movement (64).

The endothelium serves as a barrier between the blood stream and the surrounding tissues, and adherens junctions in endothelial cells serve an important role in this function by preventing leakages while allowing for vascular remodelling and the passage of solutes (67,68). Increased substrate stiffness in diseases such as atherosclerosis leads to inflammation and increased barrier permeability, resulting in adverse health effects (67). Endothelial AJs also play an important role in mechanosensing, specifically in sensing FSS (27). Increased tension on PECAM-1 at cell-cell adhesions caused by laminar flow triggers its association to vimentin, allowing force transmission from myosin to PECAM-1 (27). This increase in force leads to the activation of Src family kinases which phosphorylate VEGF receptors, activating downstream signalling cascades including the PI(3)K pathway (27). Potentially due to the link between cell-cell and cell-matrix adhesions, focal adhesions remodel in response to FSS (27).

In addition to being the site of force transmission between cells and FSS sensing, cell-cell junctions are involved in mediating cell guidance through cadherin fingers (22). These structures are present in the serrated cell-cell junctions found in migrating epithelial and endothelial cells, but not in the smooth junctions of stationary cells (22). They are polarized in the direction of cell movement, pointing away from the rear of migrating cells and are engulfed by the front of follower cells (22). The formation and orientation of cadherin fingers can be propagated between cells, suggesting a relationship between these structures and leader-follower relationships in migrating cells (22). Further, the loss of cadherin fingers resulted in a loss of coordinated movement, due to cadherin fingers' probable role in transmitting polarity orientation from leader cells to follower cells (22).

2.10 Extracellular Matrix Micropatterning

As previously discussed, cues from the cellular microenvironment affect cell migration and polarity. Notably, geometric confinement from neighboring cells or the ECM has a strong impact on these processes (15). On uniform cell culture substrates, heterogeneities in the ECM, such as in substrate stiffness or in biochemical composition, are missing, as are limitations on cell spreading area and volume (15). Micropatterns of ECM proteins allow us to provide cells with some of these important physico-chemical and geometric constraints *in vitro*, by creating micron-scale adhesive features on an otherwise non-adhesive substrate. This, in turn, lets us to control cell shape and tissue architecture through the resulting pattern of cell adhesion (15,69). Thus, micropatterning is a powerful tool for investigating the relationship between cell shape, tissue patterning and cell function (15,69). It additionally allows us to investigate the effect of spatial cues in the form of external adhesive conditions on various cell functions (70).

In order to create these micropatterns, anti-fouling regents, such as polyethylene glycol (PEG), can be used to first render the entire substrate non-adhesive (15,69). This anti-fouling coating is either selectively destroyed or selectively activated to bind ECM proteins in particular areas using different methods (15). Alternatively, select adhesive areas are first created and the surrounding areas are made non-adhesive using an anti-fouling reagent (15,69). The two most common micropatterning approaches are photolithography and soft lithography (69). Photolithography techniques require the controlled exposure of a non-adhesive substrate to light to create specific adhesive regions (Fig 4B). This exposure to light is often controlled using a photomask, however this can also be done by controlling illumination with a digital micromirror device (DMD) (Fig 4B). There are multiple ways of degrading the anti-fouling reagent to allow the binding of ECM proteins to areas of the coverslip exposed to light. Photosensitizers and fluorophores produce reactive oxygen species when excited by light, while UV light can be used to detach photosensitive chemical groups or detach the protein-repellant part of the anti-fouling reagent (15). Deep UV light (λ< 200nm) or concentrated light from a pulsed laser is used to circumvent the need for dedicated photochemistry, as the local plasma produced by excitation removes the cell and protein repellant properties of PEG (15). Even if deep UV light is used, the creation of photomasks, which requires the ability to fabricate photomasks, or the cost associated with purchasing photomasks are drawbacks of using this technique.

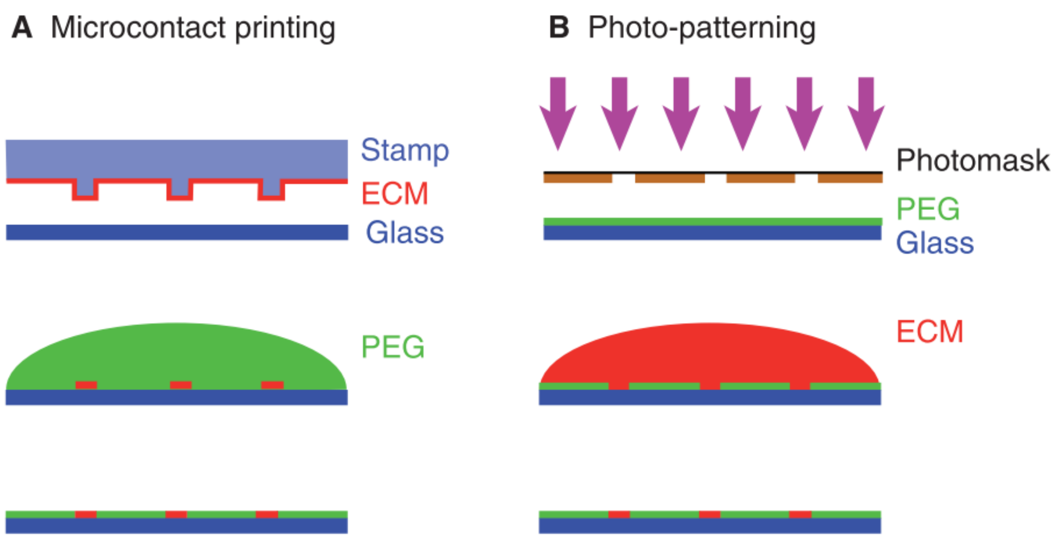

Figure 4. Commonly used micropatterning techniques. A) Workflow of microcontact printing. B) Workflow of photo-patterning. Adapted with permission from Théry, Journal of Cell Science, 2010.

Examples of soft lithography techniques include microcontact printing, microstencils, and microchannel printing (69). Microcontact printing requires the creation of a polydimethylsiloxane (PDMS) stamp by pouring un-crosslinked PDMS onto a wafer created with photolithography, and subsequently baking it to crosslink the polymer. For direct patterning, the stamp is then “inked” with ECM proteins or cell binding functional groups (Fig

4A) (69). Once the substrate has been stamped, the pattern is then backfilled with a non-adhesive reagent such as PEG (Fig 4A) (69). While the creation of the stamp is technically challenging, it can be reused for future experiments, thus simplifying the process. Other disadvantages of using this technique are the variability of the micropatterns created and the constraints imposed by the deformability of PDMS (15,71). Microchannel printing once again requires a wafer generated through photolithography (69). In this case, the wafer is used to generate a microchannel network that will deposit protein solutions in the desired pattern (69). Finally, microstencils made from PDMS sheets with holes of the desired geometries can be used to create cell islands (69). Peeling this stencil then releases the seeded cells from their confinement. While this technique does not require the fabrication of a wafer using photolithography, it does not allow the creation of micron scale features for the seeding of single cells (69).

2.11 Studying Cell Polarity and Migration Using Micropatterns of Extracellular Matrix

Given that geometric confinement has such a strong impact on cellular architecture, micropatterning can be used to study a variety of biological processes, including cell division, growth, differentiation, polarity and migration (15). To confine single cells and force them to adopt a given shape, micropatterns must be smaller than the spreading area of the cell type used (69). Micropatterns slightly larger than the size of a given cell can be used to restrict their movements and influence their morphology while not dictating it as such. Larger micropatterns, several times larger than the size of a single cell, can be used for the study of multicellular islands, which do not directly control the shape of individual cells but might influence it, nonetheless (69).

Micropatterning influences the organization of the cell's cytoskeleton through the distribution of cell-matrix adhesions (15). Binding of ECM fibers by transmembrane proteins, such as integrins, induces localized signalling and cytoskeletal assembly (15). The distribution of focal adhesions has been shown to affect the spatial organization of stress fibers in cells plated on micropatterns, with anisotropic micropattern shapes leading to the anisotropic distribution of focal adhesions and, as such, an anisotropic distribution of stress fibers (15). This important effect of micropattern shape on cell architecture has further been shown to affect cell polarity. A study by Théry et al. demonstrated that plating cells on anisotropic patterns influences microtubule organization in addition to that of the actin cytoskeleton (14). The internal organization of the cell was also found to be affected, with the nucleus-centrosome polarity axis of cells of a given area depending on the shape of the micropatterns they were seeded on (14).

Imposing a given shape on a cell can increase the likelihood of observing certain behaviours of interest compared to a uniform 2D substrate, as cell behaviour on these substrates is highly heterogeneous. In fact, imposing a polarized shape on cells using micropatterns can influence the likelihood of them migrating, as well as the direction they migrate in. Cells seeded onto micropatterned teardrop shapes to induce polarization were found to migrate in the direction of their blunt end when confinement was released (72). In addition, cells seeded onto triangular "ratchets" with gaps of varying sizes between them were found to be more likely to migrate towards the narrow end of the micropattern when the gap was larger (73). This bias in directionality was a result of the larger area accessible to protrusions for the nucleation of new focal adhesions on the adjacent pattern (73).

Micropatterns can also be used to study collective cell migration. A study by Jain et al. has provided novel insight on cell polarization during collective cell migration. Cells seeded at the appropriate density on micropatterned rings form trains of cells which undergo collective rotational movement (74). Front-rear polarity at the level of individual cells was found to be important for the maintenance of this collective movement, acting through cryptic lamellipodia which serve to maintain the coordination of polarization in these cells (74). Stencil-based micropatterning has also been used to study the emergence of leader cells during collective migration (75). Removal of the stencil triggered collective migration, thus allowing reproducible traction force and monolayer stress measurements (75).

This brief review illustrates the advantages of using micropatterns for the study of cell migration, specifically with regards to reproducibly generating behaviours of interest and investigating the effect of geometric cues on migrating cells.

2.12 Morphometrics

Cell shape is mainly determined by cytoskeletal and membrane dynamics, but can also be influenced by confinement from the extracellular matrix or neighbouring cells (29). Cells can use a variety of different types of protrusions for migration, such as lamellipodia, filopodia and blebs, all of which have distinct shapes (29). The type of protrusion a cell employs can be used to determine which migration mode it is using, with amoeboid migration typically being bleb or pseudopod-based and mesenchymal migration being lamellipodia-based (29). Considering the shape of an entire cell, instead of simply looking at the shape of the protrusion can also be informative, as given cell types tend to favour certain shapes (29). In fact, performing a morphological analysis on migrating cells has suggested that their choice of cell shape is constrained by intrinsic and environmental factors, and that these cells cannot simply adopt an arbitrary morphology (29).

Morphometrics, the quantitative analysis of form, is an important tool for the study of cell migration and the biological processes in which it is involved, including morphogenesis and cancer metastasis (76,77). Single-cell morphometrics has been used to predict the metastatic potential of cells (76). In this study, the morphological features associated with increased ploidy were found to be distinct and heritable and, as such, these features could be used to predict the tumorigenic and metastatic potential of multiple mouse models of breast cancer *in vivo* (76).

Traditionally, morphometric analysis begins with cell segmentation, which outputs a binary mask of the cell being analyzed (29). Next, cell shape is quantified using standard geometric features, landmark points on the cell outline which uniquely define its shape or Fourier descriptors (29). Standard geometric features for 2D cells include area, perimeter, and circularity (29). Fourier descriptors are obtained from the Fourier transform of the x and y components of the cell outline (29). Finally, this high dimensional data is analyzed using dimensionality reduction techniques such as Principal Component Analysis (PCA) or t-distributed stochastic neighbor embedding (tSNE) (29). Sub-populations of cells with distinct shapes can be identified visually or, more quantitatively, using clustering algorithms (29). One can further predict to which subpopulation a given cell will belong using algorithms such as decision trees or Bayes classifiers (29). As an alternative to segmentation and feature extraction, deep learning tools can be used to classify cells into subpopulations (29).

Analyzing the shape of migrating cells has unveiled several interesting relationships. Keren et al. found that the shape of migrating keratocytes fit into one of two broad categories: canoe-shaped cells or D-shaped cells (78). They further found that cell speed could be predicted from a cell’s aspect ratio, as more elongated cells have a less curved lamellipodium leading to the presence of larger area with high actin density (78). The high actin density region was responsible for pushing the cell membrane forward at a faster rate than in more curved areas (78). In a different study, analysis of *Dictyostelium* amoebae migrating in microfluidic chambers with chemotactic gradients of different steepness revealed that the amoebae adopted different shapes depending on how noisy the gradient was (79). Cells migrating along gradients with a high signal-to-noise ratios were highly elongated whereas cells migrating along low signal-to-noise ratios were less elongated overall, going through cycles of forming split pseudopods to perform a biased random walk along the gradient, followed by periods of elongation (79). Cells on noisier gradients additionally had more variability in shape (79). While these studies clearly demonstrate that cell morphology and migration are linked, our knowledge of their relationships is still limited.

3 METHODS

3.1 Micropatterning

Micropatterning was done using the Micropatterning Fabrication Kit from 4DCell (MP-K), which provided a protocol and some materials. 25mm round glass coverslips (4D Cell or Electron Microscopy Sciences, catalog #72290-12) were cleaned with 70% ethanol and Kimwipes. The coverslips were then activated for 10 minutes under deep UV in a deep UV/Ozone cleaner (Fig 5A) (Bioforce PC440.110V). Each coverslip was incubated for 30 minutes, activated side down, on drops of the anti-fouling reagent PLL-PEG, at a concentration of 0.1 mg/mL (4D Cell or SuSoS, #PLL (20)-g[3.5]- PEG(2)), placed on parafilm (Fig 5A). After incubation, each coverslip was washed with deionized water and air-dried coated side facing up. Once dry, coverslips were placed on the desired quartz photomask (4DCell) and kept in place with a photomask holder (4DCell). Photomasks to create lines or circles 10-100 µm in width or diameter, respectively, were used. The photomask and coverslip were placed in the deep UV/ozone cleaner for 10 minutes (Fig 5A). Next, the coverslips were detached using deionized water and subsequently air-dried. They were then incubated with a solution of extracellular matrix (ECM) protein on parafilm for 30 minutes (Fig 5A). The ECM protein mix was made up of 25% fibronectin (4DCell or Sigma-Aldrich, catalog #F1141-1MG) at a concentration of 50 µg/mL, 25% AF647-conjugated fibrinogen (Fisher Scientific, catalog #F35200) at a concentration of 20 µg/mL and 50% 1X PBS (Corning, catalog #MT2104CV). Once the incubation was finished, the coverslips were washed on drops of deionized water on parafilm. Finally, coverslips were stored floating patterned side down on PBS with an antimicrobial agent, Antibiotic-Antimycotic (anti-anti, Thermo Scientific, catalog # 15240062), in 6 well plates at 4°C for up to 2 weeks.

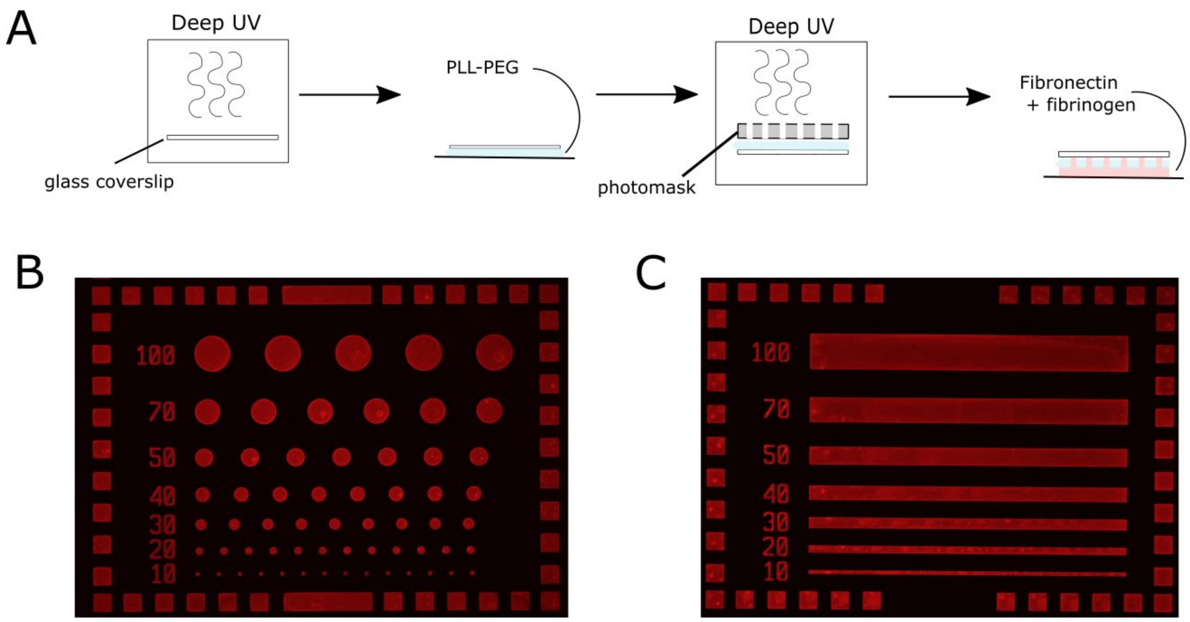

Figure 5. Generating micropatterns of ECM proteins. A) Schematic of micropatterning workflow. B) Example of micropatterned circles generated. C) Example of micropatterned lines generated. B, C) Number next to micropatterns indicate diameter (for circles) or width (for lines).

3.2 Cell Culture

hTERT-immortalized HUVECs (HT73) (22) with different fluorescent probes were maintained in EndoGro-VEGF Complete Culture Medium (Millipore Sigma, catalog #SCME002) and the appropriate antibiotics in order to maintain transgene expression. The antibiotics (Invivogen) used for each cell line were as follows:

Cell line	Antibiotic	Working Concentration	Catalog #
HT73	Hygromycin B gold	50 µg/mL	Ant-hg-1
DORA-RhoB	Blasticidin	10 µg/mL	Ant-bl-1
Raichu-Rac	Blasticidin		
Ftractin-mRuby3	G418	0.5 mg/mL	Ant-gn-2
VE-cadherin-mRuby3	Puromycin	0.5 µg/mL	Ant-pr-1

Table 1. Antibiotics used for cell culture maintenance.

Corning Cell Culture 1X PBS (Fisher Scientific, catalog #MT2104CV) and Corning 0.05% Trypsin-EDTA (Fisher Scientific, catalog #25300054) were used for cell passaging.

All HUVEC lines used were made by lentiviral transduction, using lentiviral particles produced in HEK293FT cells. These cells were maintained in DMEM (Dulbecco's Modified Eagle Medium) (Fisher Scientific, catalog #11965092) supplemented with 10% FBS. PBS and trypsin, as described above, were used for passaging these cells.

3.3 Microscopy

All images were acquired on a fully automated Nikon Ti2 widefield epifluorescence microscope system equipped a multispectral LED light source (Lumencor SpectraX), a Perfect Focus System (PFS), a motorized stage, a sCMOS camera (Hamamatsu Orca FusionBT or Photometrics PrimeBSI), an incubation chamber (Digital Pixel), and controlled by Nikon NIS-Elements HC. In experiments where cells expressing the DORA-RhoB FRET probe were used, images were acquired with a CFI Plan Apo 20x 0.75 NA objective and no binning. In experiments where cells expressing the Raichu-Rac probe were used, a CFI Plan Fluor 40x 1.3 NA oil-immersion objective and 2x2 binning were used. The optical configurations used for experiments were:

Multichroic mirror	Emission Filter (nm)	Excitation filter (nm)	Used for
Chroma 89007bs	473/24	440/20	FRET (CFP) when combined with mRuby3 imaging
Chroma 89007bs	535/30	440/20	FRET (YFP-FRET) when combined with mRuby3 imaging
Chroma 89007bs	600/50	555/10	mRuby3, alone and when combined with CFP and YFP-FRET
395/470/550/640	705/72	640/30	AF647
458	535/30	440/20	YFP-FRET alone, or combined with AF647

Table 2. Optical Configurations for Imaging.

All cells were imaged in Live-cell Imaging Solution (LIS), a HEPES-buffered live-cell imaging medium with low background fluorescence (22). It is composed of extracellular buffer (ECB), 1% FBS and 5 ng/mL bFGF. ECB contains 20 mM HEPES, milliQ water, 5 mM KCl, 125 mM NaCl, 1.5 mM $MgCl_2$, 1.5 mM $CaCl_2$ and 10 mM D-glucose. Once the ECB is made, its pH is adjusted to 7.4 and it is sterile filtered. After this, the previously mentioned supplements can be added, and the LIS can be stored at 4°C for up to 1 month.

3.4 Live Cell Imaging of Cells on Micropatterns

All live-cell imaging experiments were performed at 37°C. Micropatterned coverslips were placed in magnetic coverslip holders (Live Cell Instruments, catalog #CM-B25-1), and exposed to UV light for 15 min to sterilize them ahead of cell seeding. Cells were seeded in full growth medium and left to attach overnight. For behavioural quantification experiments, 5000 cells were seeded onto coverslips with micropatterned lines, and 14 000 cells were seeded onto coverslips with micropatterned circles. For all other experiments, cells were seeded at a density of 14 000-17 000 per coverslip with micropatterned lines and at a density of 58 000 cells per coverslip with micropatterned circles. For all experiments, cells were seeded in full growth medium containing an antimicrobial cocktail (anti-anti). The day of imaging, the growth medium was replaced with Live Imaging Solution (LIS) containing anti-anti. The coverslip holder was placed on the microscope 1 hour before the start of imaging for thermal equilibration (37°C). For cells on lines images were acquired at a rate of 1 frame/minute and for cells on circles images were acquired at a rate of 1 frame/25 seconds. Images were acquired for a total of 30 minutes for behavioural quantification experiments, and for two hours for other experiments with cells on micropatterned lines. Blebbing cells were imaged at 3 second intervals for a total of 300 seconds. The cell lines imaged on micropatterns were HT73 DORA-RhoB and HT73 Raichu-Rac Ftractin-mRuby3.

3.5 Live Cell Imaging of Mosaic Monolayers

All live-cell imaging experiments were performed at 37°C. Glass bottom 96-well plates (Cellvis, catalog #P96-1.5H-N) were coated with 1:100 bovine collagen solution (Cedarlabe Labs, catalog #5005-100ML) diluted in PBS (Fisher Scientific, catalog #10-977-015) and incubated at 37°C for 2-4 hours. Plates with collagen coated wells were stored with PBS at 4°C for a under two weeks before use. Cells were seeded at a density of 20 000/well 24 hours before imaging, with 1:20 cells expressing DORA-RhoB or Raichu-Rac and the remaining cells expressing VE-cadherin mRuby3. Cells were seeded in media containing anti-anti. The day of imaging, growth medium was replaced with LIS containing anti-anti and the 96-well plate was placed on the microscope 1 hour before the start of imaging for thermal equilibration (37°C). Images were acquired at a rate of 1 frame/minute over 2 hours. Plates were sealed shut using PolarSeal Aluminum Microplate Seals (Thomas Scientific, catalog#1152A34).

3.6 FRET

Cells expressing the unimolecular DORA-RhoB probe were used to investigate Rho signalling. This probe was introduced by Reinhard et al., and consists of the Rho binding domain of PKN1 (ΔPKN), mVenus, Cerulean3 and Rho B (Fig 6A) (80). When Rho B binds to GTP, the conformational change induced results in higher FRET efficiency (Fig 6A) (80).

Cells expressing the unimolecular Raichu-Rac probe were used to investigate Rac signalling. This probe was introduced by Itoh et al., and consists of YFP, PAK1, Rac1 and CFP (Fig 6B) (81). Upon GTP loading of Rac1, the resulting conformational change leads to a higher FRET efficiency (Fig 6B) (81).

Ratio-metric FRET was performed by computing the ratio of intensities in the YFP-FRET and CFP channels. Before this ratio was calculated, the images were background-subtracted, sub-pixel aligned, and jitter corrected. Cells within each field of view were masked using histogram-based segmentation, and only the ratios within masked areas are stored. Once ratios were calculated for each frame, they were then corrected to account for photobleaching.

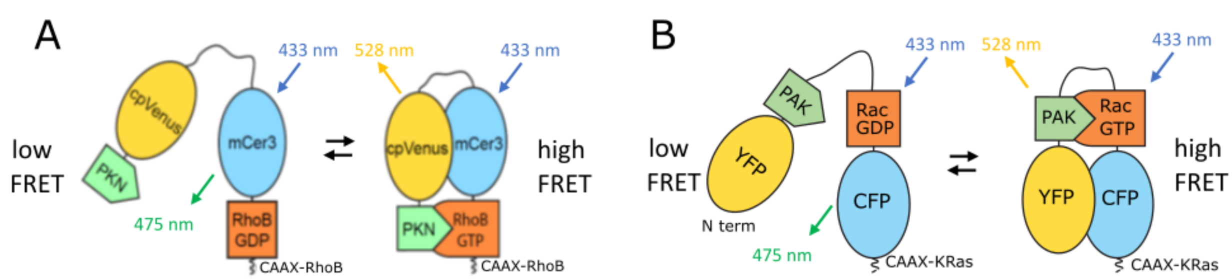

Figure 6. FRET probes. A) Design of DORA-RhoB FRET probe. B) Design of Raichu-Rac FRET probe. A, B) Diagrams made by Dr. Arnold Hayer.

3.7 Cell Edge Window Analysis

Using custom MATLAB code (8), the edge of each segmented cell was divided into 180 evenly-spaced coordinate windows, which go 3 µm inside the cell. For each frame, the edge velocity was computed in each window, as was the average FRET activity, allowing us to visualize each of these as a function of time. This allowed us to compare Rho GTPase activity in protrusions and retractions. The relationship between edge velocity and Rho GTPase activity was quantified using cross-correlation analysis.

3.8 Rho GTPase Buildup and Decay

The relationship between edge velocity and Rho GTPase activity was further characterized by calculating the lags between the start of Rho activity buildup and the onset of retraction, between the start of Rac activity buildup and the onset of protrusion, between the start of Rho activity decay and the onset of protrusion and between the start of Rac activity decay and the onset of retraction. These lags are calculated from traces of the mean edge velocity and mean Rho GTPase activity within a selected protrusion-retraction cycle. The reference points used in calculations (i.e., onset of retraction, start of Rac activity buildup) were determined visually. The onset of protrusion was considered to be the approximate point when edge velocity switched from negative to positive and the onset of retraction was considered to be the approximate point when edge velocity switched from positive to negative. The start of Rho GTPase buildup was considered to be the point from which a fast buildup of GTPase activity was observed after minimum activity was reached, and similarly, the start of Rho GTPase decay was considered to be the point from which a fast decay of GTPase activity was observed after the peak activity had been reached.

3.9 Rho GTPase Gradient Analysis

For both autonomously migrating and collectively migrating cells, we calculated the steepness of the back-to-front gradient of Rho activity within a peripheral ring using custom code. This peripheral ring was 4 µm wide for autonomously migrating cells and 3 µm wide for collectively migrating cells. After creating the mask, Rho activity was averaged along the length of the cell, which was then standardized to a create a 201x1 vector for each frame. The vectors were averaged to obtain an average of Rho activity along the cell length over time. A linear fit was performed on this trace and the slope of this line was taken to be the steepness of the gradient. This process was repeated for Rac in collectively migrating cells. For collectively migrating cells, cells were additionally rotated to account for changes in their direction while they migrate.

3.10 Morphometrics

To obtain information on the morphology of cells plated on micropatterned lines and cells in monolayers, we used a Cell Profiler pipeline provided along with VAMPIRE, an unsupervised machine learning algorithm which uses the shape of the cell outline and Principal Component Analysis features to identify example cell shapes within the population (82). Through this Cell Profiler pipeline, we were able to determine the cell area, major axis length and aspect ratio for each cell (82). For this, cropped images, most often only containing one cell were segmented and data was automatically extracted was saved as a csv file.

3.11 Computational Determination of Cell Motility Parameters

Using a custom MATLAB script, the centroid of all cells of interest was determined and tracked over the course of imaging. The coordinates of the centroids of segmented cells were calculated and the cell's net displacement was calculated as the distance between the coordinates of its centroid in the first and last frames. A cell's average velocity was calculated as the mean of the displacement between each frame and the next. Finally, a cell's persistence was calculated as the ratio of net displacement and total displacement.

3.12 Spatial Propagation of Rho GTPase activity

Rho GTPase activity in cells with periodic protrusion-retraction cycles on 20 and 30 μm patterns was averaged along the entire cell length for each frame, into a 201x1 vector. From the top 10% of the values from the resulting matrix, the extent of spatial propagation was estimated as a percentage of cell length.

3.13 Data Visualization

Swarm plots with notched lines representing the median and the 25th and 75th percentiles of each group featured in figure panels 10D, 11A, 11C, 11F, 11H, 11I, 15A and 15C were made using dabest, a Python package described by Ho et al. (83). Stacked bar charts were made using custom code and the Python package Matplotlib. All other plots were made using custom code and the Python package Seaborns.

4 RESULTS

4.1 Using Micropatterns of ECM Proteins for the Study of Cell Motile Behaviour

To achieve our goal of understanding the differences between autonomous and collective cell migration, we first sought to gain a greater understanding of the requirements for autonomous cell migration. We observed that HUVECs sparsely plated on a uniform substrate typically adopt a multipolar morphology, and do not undergo directional migration. In contrast, HUVECs in monolayers on uniform 2D substrates spontaneously migrate, and these cells are generally compact in shape, with a defined front and rear. As such, we were prompted to question whether there was a link between the morphologies of cells in these two contexts and their motile behaviours.

Previous studies have clearly demonstrated a connection between cell morphology and cell migration (78,79). The morphology of chemotaxing *Dictyostelium* varies based on the steepness of the chemotactic gradient (79), while the speed with which fish keratocytes migrate depends on their aspect ratio (78). However, it is not known whether similar relationships between cell shape and cell motile behaviour exist in other cell types. It is additionally unknown if controlling the adhesion geometry of cells affects their motile behaviour. We determined that micropatterns of ECM proteins provided an ideal system to generate cells with controlled variations in shape, imposed through geometric restrictions of the cell's adhesive surface.

Plating cells on micropatterned lines, we created a population with a large range of cell lengths and aspect ratios. Within this population, many cells underwent autonomous directed migration, without the need for any additional external cues. However, the majority of cells did not migrate. Instead, a large number of these non-migratory cells developed competing fronts with periodic protrusion-retraction cycles. Comparing the morphologies of these two groups of cells, we noted that migrating cells tended to be shorter in length and have smaller adhesive areas than cells with periodic protrusion-retraction cycles. This observation led us to perform a large-scale quantification of the relationship between cell morphology and cell motile behaviour, with the aim of determining whether a cell's area, length or degree of elongation impacted its likelihood of migrating in a directed manner.

4.2 Pattern Width and Cell Elongation Impact Likelihood of Directed Migration on Micropatterned Lines of Extracellular Matrix

As mentioned in the section above, cells plated on micropatterned lines could broadly be divided into two group, migrating cells and non-migrating cells. The majority of migrating cells observed were smaller and shorter than the average cell, which did not migrate. This led us to hypothesize that the likelihood of a given cell undergoing directed migration depends on its size and shape. We thus decided to perform a quantification of cell motile behaviour on micropatterned lines of ECM proteins, and to determine if any meaningful relationship between cell morphology and the likelihood of migration exists.

To systematically quantify the relationship between micropatterned line width, cell shape, cell size and a cell's migratory phenotype, we seeded cells onto micropatterned coverslips at a density such that we obtained roughly one cell per line in each field of view. We imaged HT73 DORA-RhoB HUVECs plated on 20-70 μm-wide micropatterned lines at 1-minute intervals for 30 minutes. We used the DORA-RhoB probe as a membrane marker, which allowed us to segment cells as part of the computational analysis of their morphology and motility. Only cells which did not touch other cells or the end of a micropatterned line, and which remained in contact with the edges of the micropattern during imaging were considered in our analysis. The analysis of cell shape parameters was conducted using VAMPIRE, a computational tool which segments cells, calculates several key morphological parameters, and further has the capacity to classify cells into "shape modes" based on the shape of their outlines (82). With VAMPIRE, we were able to obtain the length, area, and aspect ratio of each of the cells analyzed. We considered cell length to be the length of the major axis and aspect ratio was calculated as the ratio of major axis length to minor axis length. For our analysis of cell motility, we computed the net displacement by calculating the distance between the cell centroid in the first and last frame. We further calculated the directional persistence of its migration by dividing the net displacement of the cell centroid by its total displacement, which was calculated as the sum of centroid displacements between each frame and the next.

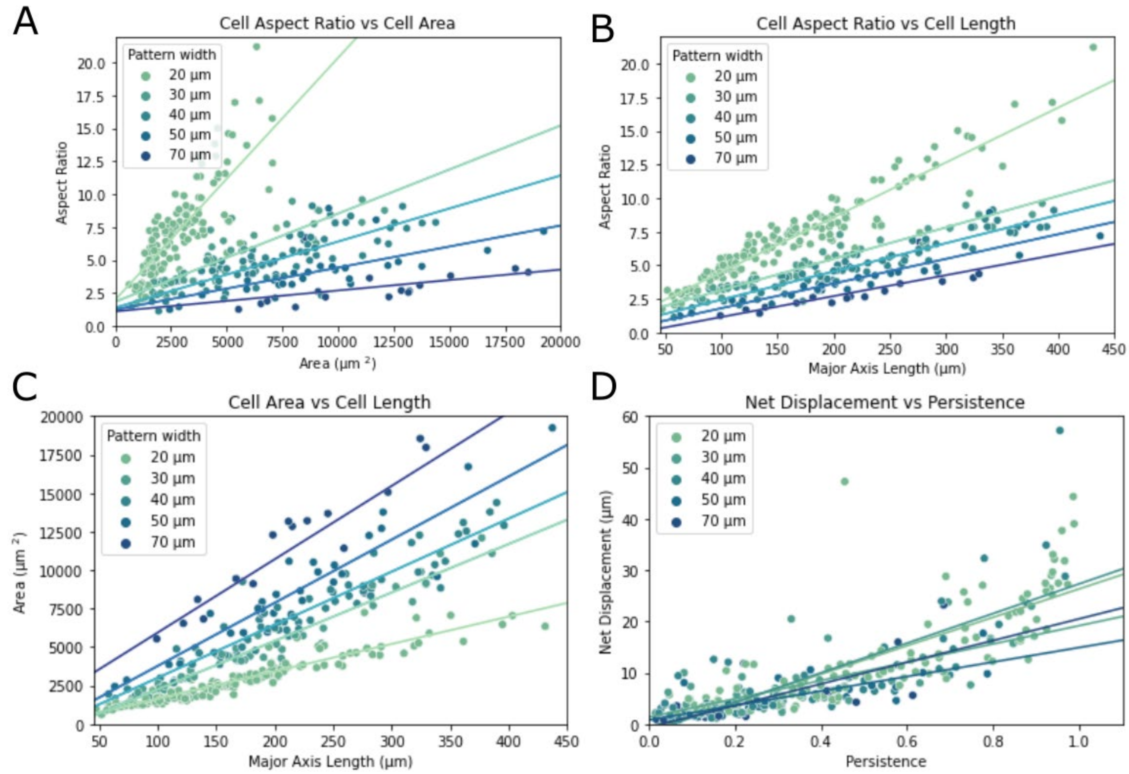

Figure 7. Analysis of morphology and motility for cells plated on micropatterned lines. HT73 DORA-RhoB HUVEC were seeded onto coverslips with micropatterned lines of fibronectin and AF-647 conjugated fibrinogen. Cells on 20 µm, 30 µm, 40 µm, 50 µm and 70 µm micropatterned lines were imaged at 1-minute intervals for 30 minutes. A) Cell aspect ratio as a function of cell area. B) Cell aspect ratio as a function of cell length. C) Cell area as a function of cell length. D) Net displacement as a function of migration persistence. A-D) 317 cells from 3 trials, fit lines for each pattern width calculated using linear regression. Each dot represents one cell.

It is important to note that the number of cells that could be analyzed decreased as pattern width increased because the portion of the cell population with a sufficiently large area to cover the entire width of the micropattern was lower. It is also important to note that for a given pattern size, cells with a larger area would also be longer and have a higher aspect ratio. However, if cells have roughly the same area but are on micropatterns with different widths, the cells on narrower micropatterns would be longer and have higher aspect ratios. Our analysis of cell morphology revealed that for all pattern widths, cell aspect ratio scaled linearly with cell area (Fig 7A). Cell aspect ratio and cell area also scaled linearly with cell length (Fig 7 B, C). Further, net displacement scaled linearly with persistence when persistence was between 0 and ~0.9 (Fig 7D). The variation in net displacement for persistence scores between ~0.9 and 1 was likely due to differences in cell speed (Fig 7D).

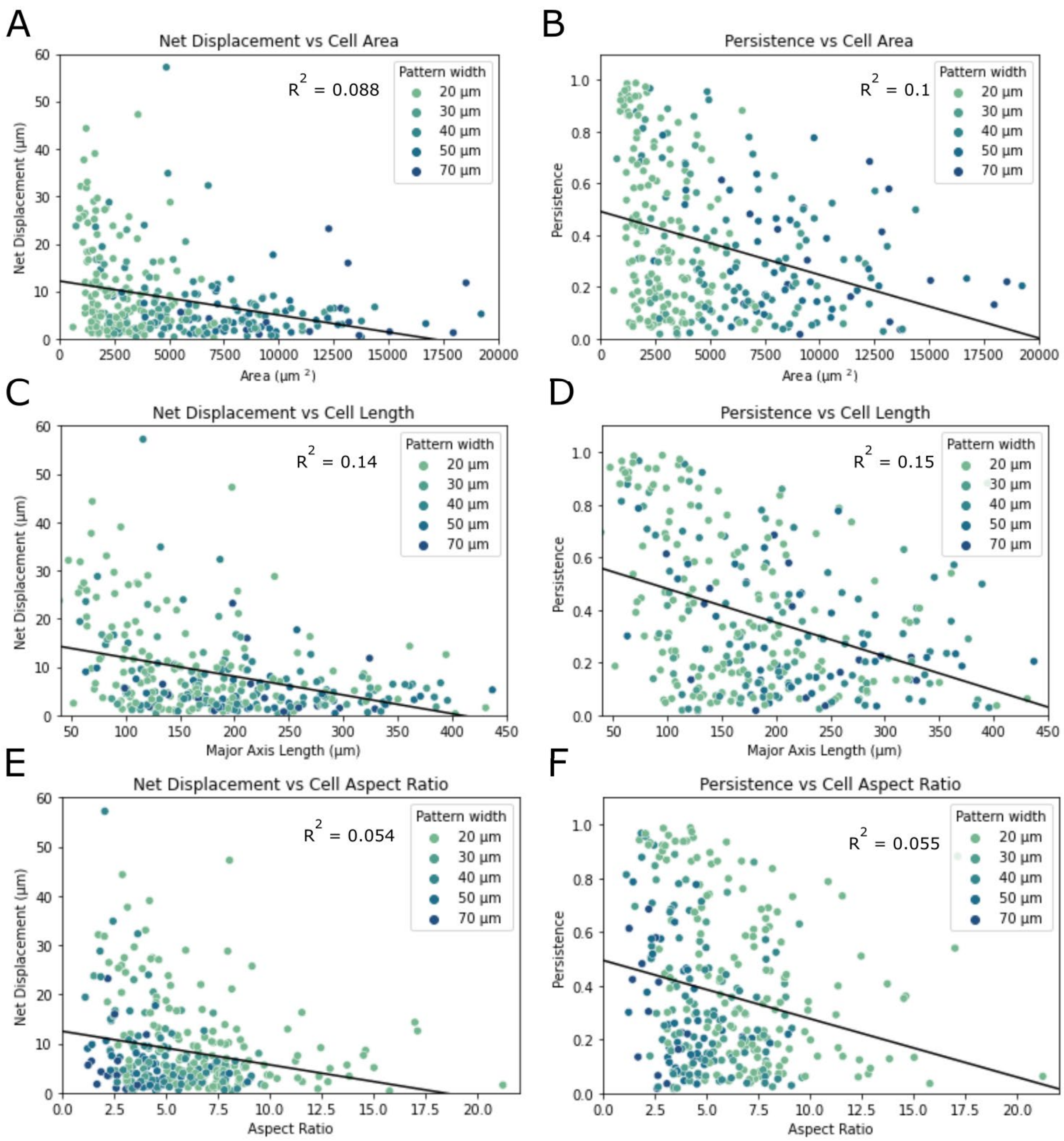

Figure 8. Cells with increased area, length and aspect ratio migrate lesser distances. Cells on 20 µm, 30 µm, 40 µm, 50 µm and 70 µm micropatterned were imaged at 1-minute intervals for 30 minutes. A) Net displacement as a function of cell area. B) Persistence as a function of cell area. C) Net displacement as a function of cell length. D) Persistence as a function of cell length. E) Net displacement as a function of cell aspect ratio. F) Persistence as a function of cell aspect ratio. A-F) 317 cells from 3 trials, fit lines (in black) calculated using linear regression. Each dot represents one cell.

By relating morphological data to net displacement, we showed that larger and longer cells, with a higher aspect ratio, tended to migrate a lesser distance (Fig 8A, C, E). Smaller, shorter cells, with a lower aspect ratio had a broader distribution of distances migrated (Fig 8A, C, E). Repeating this analysis with persistence, we found that larger, longer cells with a higher aspect ratio tended to migrate less persistently (Fig 8B, D, F). However, there was far more variation in the persistence of smaller, shorter cells with a lower aspect ratio (Fig 8B, D, F).

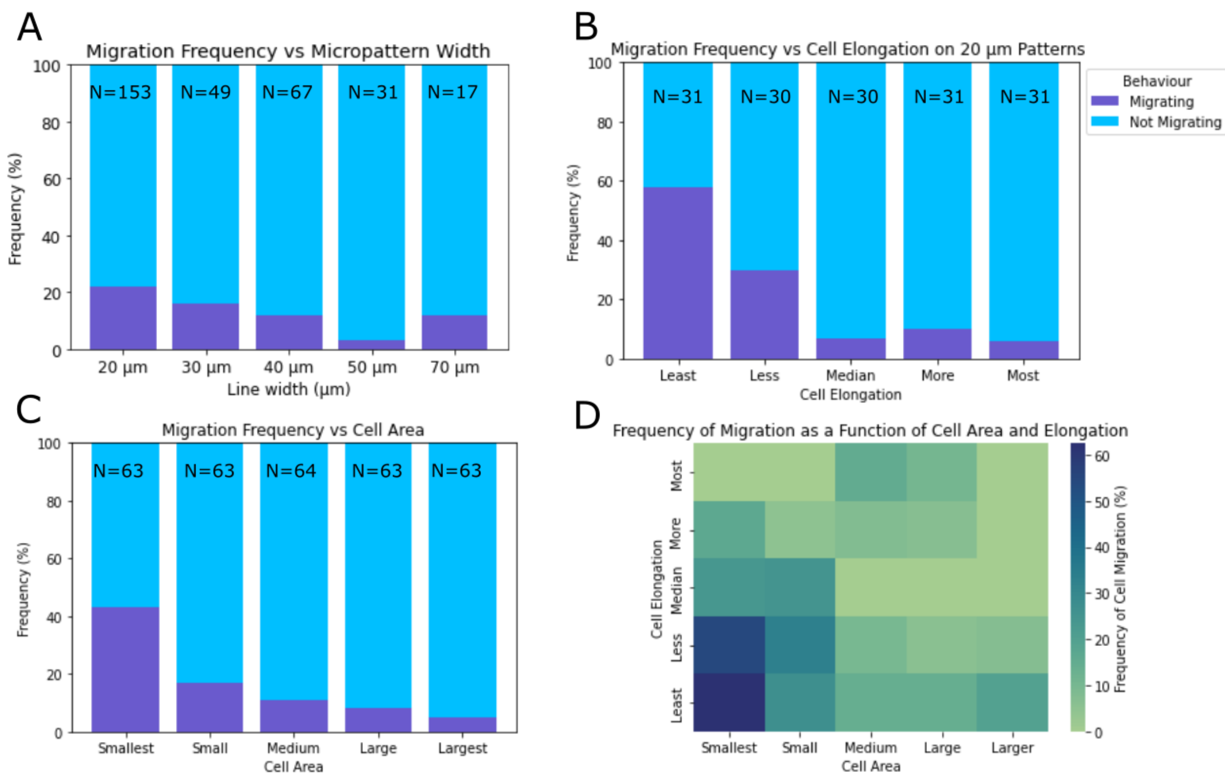

Figure 9. Cell elongation and cell area contribute to the likelihood of a given cell migrating. Cells on 20 µm, 30 µm, 40 µm, 50 µm and 70 µm micropatterned were imaged at 1-minute intervals for 30 minutes. A) Migration frequency as a function of micropattern width. Migrating cells were those that migrated 15 µm or more over the course of imaging, 317 cells from 3 trials B) Migration frequency as a function of cell elongation, 153 cells from 3 trials. Aspect ratio (AR) was used to categorize cells into 5 bins, each containing roughly ~20% of cells on 20 µm-wide micropatterned lines, as follows. Smallest cells: AR<4.4, Small cells: 4.4<AR<6, medium-sized cells: 6<AR<7.5, large cells:7.5<AR<8.7615, largest cells: 8.7615<AR. A-G) 317 cells from 3 trials. C) Migration frequency as a function of cell area, 317 cells from 3 trials. Area was used to categorize cells into 5 bins, each containing roughly 20% of the cell population, as follows (in µm^2). Area<1901, less elongated cells: 1901<Area<3095, cells with median elongation: 3095<Area<4933, more elongated cells: 4933<Area<8096, most elongated cells: 8096<Area. D) Migration frequency as a function of both cell area and cell elongation, 317 cells from 3 trials. Same area bins were used as in C. 5 aspect ratio bins, each containing 20% of the cell population were defined as follows. AR<3.39, less elongated cells: 3.39<AR<4.584, cells with median elongation: 4.584<AR<6.16, more elongated cells: 6.16<AR<7.87, most elongated cells: 7.87<AR.

To elucidate the contributions of pattern width and cell shape parameters to cell motility more easily, we classified cells as "migrating" and "non-migrating". Based on the distribution of cell displacement, we considered that all cells with a net displacement of 15 µm or greater in 30 minutes would make up the group of migrating cells, while the remaining cells were classified as non-migrating. We observed that cells tended to migrate more frequently on narrower patterns, with the proportion of migrating cells being highest for 20 μm-wide micropatterned lines (Fig 9A). We additionally quantified the relationship between cell elongation and likelihood of migration for cells plated on 20 μm-wide micropatterned lines. We divided cells into bins based on their aspect ratio, or elongation, with each bin containing 20% of the cell population and calculated the proportion of migrating cells for each group. Shorter cells were considerably more likely to migrate, with 58% of the "least elongated" cells and 30% of the "less elongated" cells having a net displacement over 15 μm (Fig 9B). All other groups had 90% or more cells in the non-migrating category (Fig 9B).

To determine the contribution of cell area irrespective of pattern width, we divided the entire population of cells into 5 bins based on cell area. Cells with the smallest area were most likely to migrate, and the likelihood of a cell migrating decreased as its area increased (Fig 9C). Further, by binning cells into 5 groups by area and 5 groups based on aspect ratio, we determined that both cell area and cell aspect ratio contribute to the likelihood of a cell migrating (Fig 9D). The effect of these parameters can be combined, as the group of cells most likely to migrate are the smallest cells with the least elongated shape (Fig 9D). However, cells of all areas were more likely to migrate when they had a less elongated shape, which suggests that cell elongation might have a stronger impact on the likelihood of directed migration than cell area (Fig 9D).

Using micropatterned lines of ECM proteins, we were able to reliably generate autonomously migrating cells. This finding opens the door for a more quantitative study of this process in HUVECs, which has thus far been limited by the heterogeneity of cell behaviours on uniform 2D substrates. Our results demonstrate that restricting cell width increased the likelihood of a given cell migrating, with cells most likely to migrate on 20 μm-wide micropatterned lines. Additionally, cell area, length and elongation can be used to predict which cells are more likely to migrate. Both cell area and cell aspect ratio contribute to the likelihood of directed migration, and cells with both small areas and small aspect ratios were most likely to migrate. As such, when seeking to image cells on micropatterned lines it is best to choose smaller and less elongated cells plated on 20 μm-wide patterns. However, micropattern width and cell shape do not completely explain migratory phenotype, as a sizable proportion of cells fitting that description did not migrate.

4.3 Cells with Periodic Protrusion-Retraction Cycles Have Tightly Regulated Oscillatory Rho GTPase Signalling Dynamics

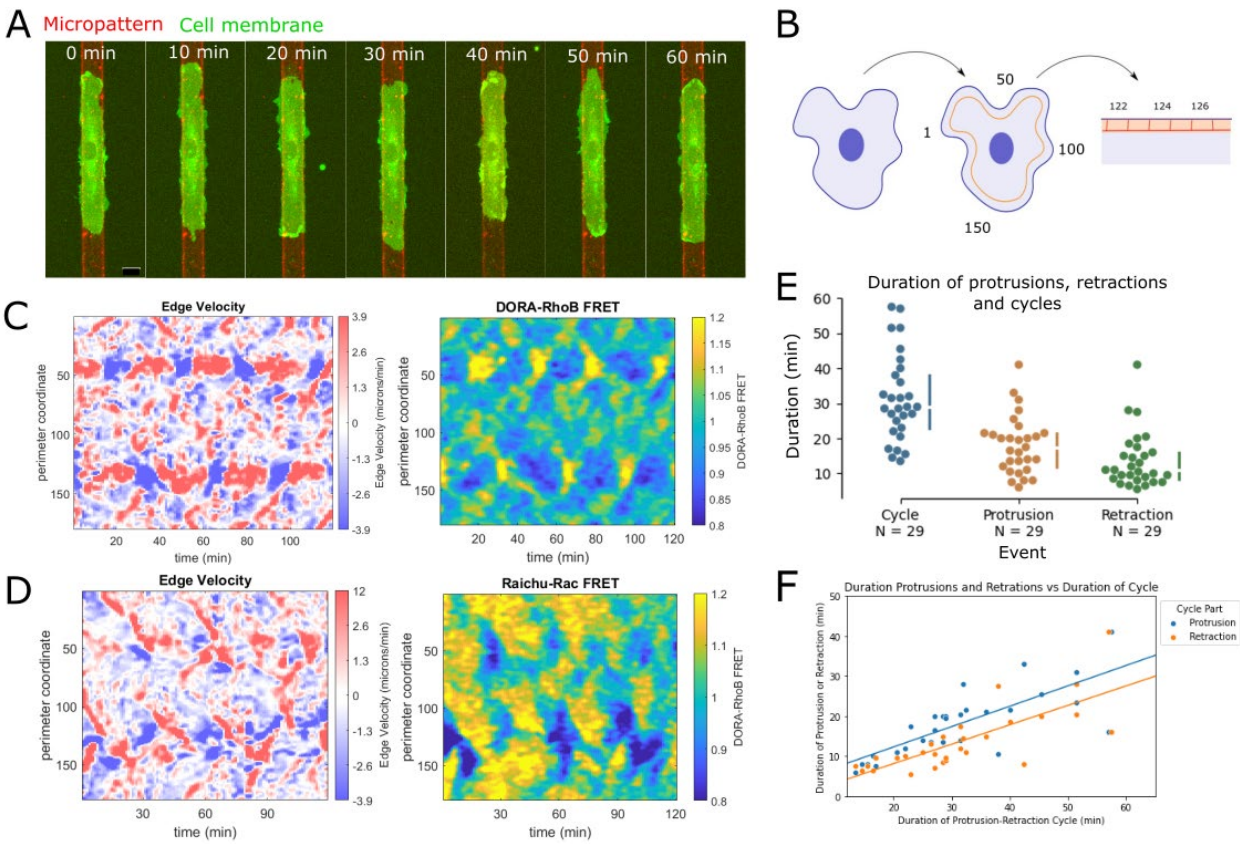

Figure 10. Cells with protrusion-retraction cycles have oscillatory Rho GTPase dynamics. A) Example of HUVEC with protrusion-retraction cycles on micropatterned lines, representative of 26 cells from 3 trials. Cell expressed DORA-RhoB as a membrane marker, micropatterns are visualized using AF647-conjugated fibrinogen, scale bar = 20 µm. B) Illustration of edge-window coordinate/perimeter coordinate numbering. C) Edge velocity and Rho activity maps for cell in A, representative of 26 cells from 3 trials. D) Example edge velocity and Rac activity maps for cell with periodic protrusion-retraction cycles, representative of 32 cells from 3 trials. E) Quantification of protrusion-retraction cycle, protrusion and retraction durations. Data from only one cycle, protrusion or retraction event per cell shown. Notched lines represent median and 25th and 75th percentiles of each group. F) Duration of protrusions and retractions as a function of cycles length. C-D) Edge velocity and Rho GTPase activity maps at edge depth of 3 µm, windows labelled clockwise starting at leftmost point. E-F) Data from 27 cells expressing DORA-RhoB or Raichu-Rac, from 6 trials.

Many of the non-migrating cells on micropatterned lines had periodic cycles of membrane protrusions and retractions (Fig 10A). Having established a link between cell shape and the likelihood of observing directional migration, we next wished to characterize the Rho

GTPase signalling dynamics of non-migrating cells with periodic protrusion-retraction cycles. By comparing the signalling dynamics of these cells to those of migrating cells, we aimed to uncover the ways in which the Rho GTPase signalling dynamics of non-migrating and migrating cells differ.

To characterize Rho GTPase activity in cells with periodic protrusion-retraction cycles, we seeded HUVECs expressing DORA-RhoB (80) or Raichu-Rac (81) on micropatterned lines and imaged them at 1-minute intervals for 2 hours. These unimolecular FRET probes allowed us to perform ratio-metric FRET analysis, as the probes emit at higher wavelengths when the GTPases are in their active, GTP-bound form. We consider that the signalling dynamics reported by the DORA-RhoB probe are representative of the activities of both RhoA and RhoB, given that this probe has been validated in the Hayer Lab with known pathways activators of RhoA. DORA-RhoB has further been shown to have the highest dynamic range of the DORA-RhoA/B/C probes (80). As such, throughout this thesis we refer to the results obtained with these probes for RhoB and Rac1 as being broadly applicable to Rho and Rac, respectively.

The signalling dynamics of Rho and Rac are of particular interest to us, as their activities are critical for the establishment and maintenance of cell migration machinery. Rac plays an important role in cell protrusions, and Rho is similarly important for cell contractions. However, the spatiotemporal dynamics of Rho activity in protrusions, retractions and migrating cells has not clearly been established in the literature. While the signalling dynamics of Rac are better established, the antagonistic activities of Rho and Rac, as well as implications by previous studies that these GTPase have different spatiotemporal signalling properties makes them ideal candidates for further study (8,9,56).

After FRET analysis, we conducted computational analysis to relate edge velocity and Rho GTPase activity at the edge of these cells (see methods). This allowed us to compare the relationship between edge velocity and Rho GTPase activity in individual cells, as well as between cells. Such analysis has previously been used by Machacek et al. and Yang et al. (8,9). For this analysis, we divided the perimeter of the segmented cell of interested into 180 coordinate windows, numbered clockwise starting from the leftmost point (Fig 10B). For each one of these windows, we computed mean edge velocity and mean Rho GTPase activity. We then generated edge velocity and Rho GTPase activity maps. Edge velocity and Rho GTPase activities were calculated within a band extending from the cell edge to a depth of 3 μm inside the cell.

Our analysis of edge velocity and Rho GTPase activity revealed that periodic protrusion-retraction cycles were accompanied by oscillatory Rho GTPase dynamics (Fig 10C, D). Based on manual quantification from traces of average edge velocity in selected cycles (Fig 11E), we determined these cycles lasted between 13.5 minutes and 57.5 minutes with an average duration of ~ 31.5 minutes (Fig 10E), and both protrusion and retraction duration increased as cycle duration increased (Fig 10F). Protrusions lasted between and 6 and 41 minutes, with an average of ~18 minutes (Fig 10E). Retractions lasted between and 5.5 and 41 minutes, with an average duration of ~13.5 minutes (Fig 10F). Protrusions were considered as all times where edge velocity was positive, and retractions were considered as all times where edge velocity was negative within the protrusion-retraction cycles analyzed.

We quantified cell averages of Rho and Rac activity in protrusions and retractions, weighted by the size of protrusions and retractions. We showed that Rho activity was significantly higher in retractions than protrusions (Fig 11A) and that Rac activity was significantly higher in protrusions than retractions (Fig 11C). Edge velocity and Rho activity were negatively correlated, while edge velocity and Rac were positively correlated (Fig 11B, D). In both cases, there was a negative temporal lag of 2 minutes between edge velocity and Rho GTPase activities. These lags indicate that while Rho and Rac activity are clearly associated with retractions and protrusions, their activities peaked with delays relative to maximum retraction or protrusion speed, respectively. (Fig 11B, D).

To further investigate the relationship between Rho GTPase activity and edge velocity in protrusion-retraction cycles, we selected areas of the edge velocity maps containing these cycles and, for these selections, calculated the average edge velocity and Rho GTPase activity over time (Fig 11E). From these average traces, we manually determined the lags between 1) the start of Rho activity buildup and the onset of retraction 2) the start of Rac activity buildup and the onset of protrusion 3) the start of Rho activity decay and the onset of protrusion and 4) the start of Rac activity decay and the onset of retraction.

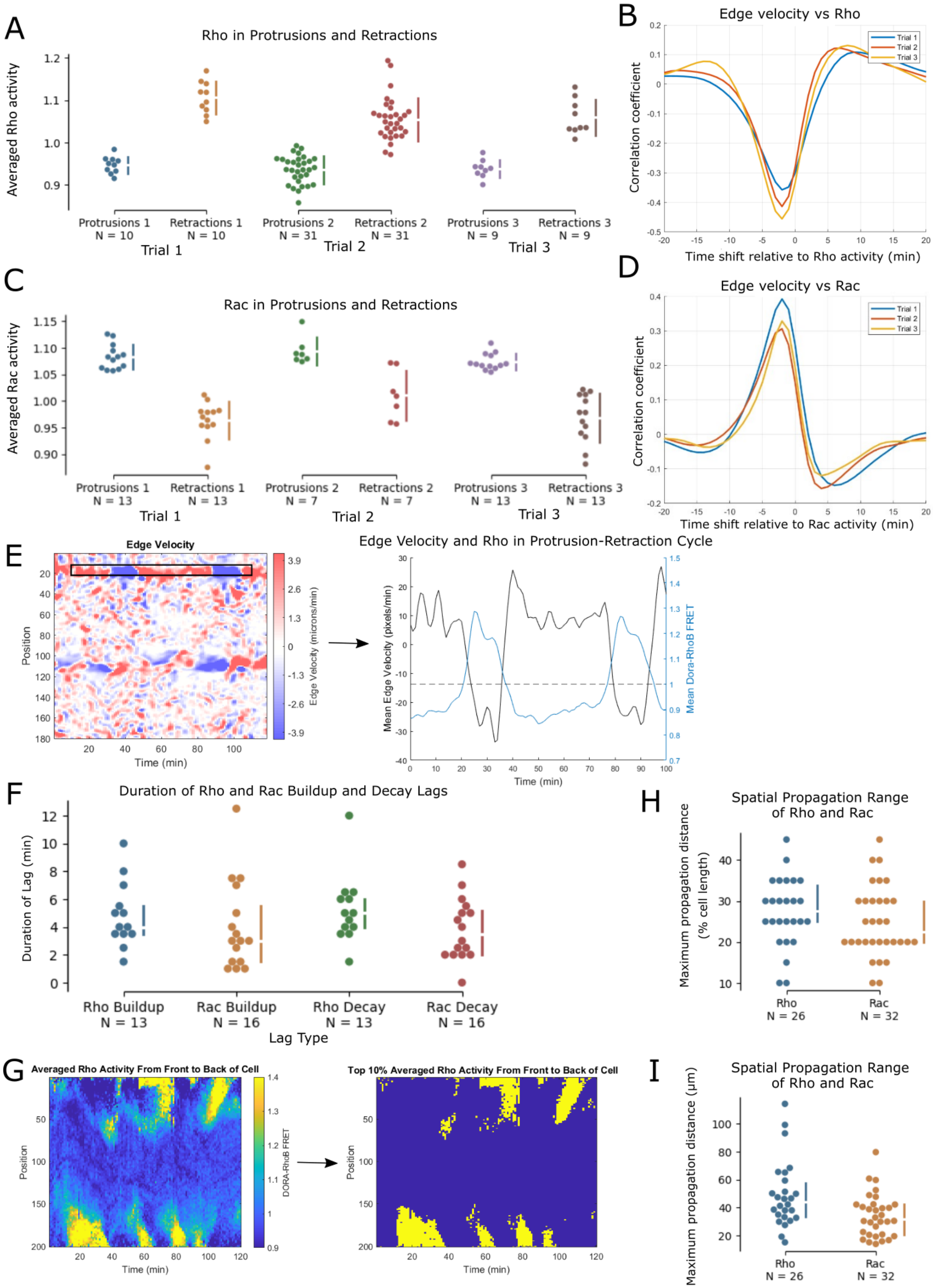
A
Rho in Protrusions and Retractions
Averaged Rho activity
Protrusions 1 N = 10
Retractions 1 N = 10
Trial 1
Protrusions 2 N = 31
Retractions 2 N = 31
Trial 2
Protrusions 3 N = 9
Retractions 3 N = 9
Trial 3
B
Edge velocity vs Rho
Correlation coefficient
Time shift relative to Rho activity (min)
Trial 1
Trial 2
Trial 3
C
Rac in Protrusions and Retractions
Averaged Rac activity
Protrusions 1 N = 13
Retractions 1 N = 13
Trial 1
Protrusions 2 N = 7
Retractions 2 N = 7
Trial 2
Protrusions 3 N = 13
Retractions 3 N = 13
Trial 3
D
Edge velocity vs Rac
Correlation coefficient
Time shift relative to Rac activity (min)
E
Edge Velocity
Position
Time (min)
Edge Velocity (microns/min)
Edge Velocity and Rho in Protrusion-Retraction Cycle
Mean Edge Velocity (pixels/min)
Mean Dora-RhoB FRET
F
Duration of Rho and Rac Buildup and Decay Lags
Duration of Lag (min)
Rho Buildup N = 13
Rac Buildup N = 16
Rho Decay N = 13
Rac Decay N = 16
Lag Type
H
Spatial Propagation Range of Rho and Rac
Maximum propagation distance (% cell length)
Rho N = 26
Rac N = 32
G
Averaged Rho Activity From Front to Back of Cell
DORA-RhoB FRET
Top 10% Averaged Rho Activity From Front to Back of Cell
I
Spatial Propagation Range of Rho and Rac
Maximum propagation distance (μm)
Rho N = 26
Rac N = 32

Figure 11. Characterization of Rho GTPase signalling dynamics in cells with periodic protrusion-retraction cycles on micropatterned lines. A) Rho activity in protrusions and retractions averaged per cell for each of the datapoints, weighted by size of protrusion and retraction events, 50 cells from 3 trials. P-values from Mann-Whitney: 1.82e-4 (trial 1), 2.74e-11 (trial 2), 4.12-4 (trial 3). B) Cross-correlation of edge velocity with Rho activity, peak lag of -2 minutes, 50 cells from 3 trials. C) Cell average of Rac activity in protrusions and retractions, weighted by size of protrusion and retraction events, 43 cells from 3 trials. P-values from Mann-Whitney: 1.6e-5 (trial 1), 5.83e-4 (trial 2), 1.6e-5 (trial 3). D) Cross-correlation of edge velocity with Rac activity, peak lag of -2 minutes, 43 cells from 3 trials. E) Illustration on selection of protrusion-retraction cycles for analysis and example of mean traces of edge velocity and Rho GTPase activity obtained for selection. F) Quantification of Rho GTPase buildup and decay lags, 13 cells from 3 trials for Rho and 16 cells from 3 trials for Rac. The Rho buildup lag is calculated as the lag between the start of Rho buildup and the onset of retraction, the Rac buildup lag is calculated as the lag between the start of Rac buildup and the onset of protrusion, the Rho decay lag is calculated as the lag between the start of Rho decay and the onset of protrusion, the Rac decay lag is calculated as the lag between the start of Rac decay and the onset of retraction. G) Illustration of data analysis for quantification of Rho GTPase spatial propagation. H) Extent of spatial propagation of elevated Rho GTPase activity relative to cell length I) Extent of spatial propagation of elevated Rho GTPase activity (in µm) H, I) 26 cells from 3 trials for Rho and 32 cells from 3 trials for Rac.

We found that the buildup of Rho activity precedes the onset of retraction by on average 4.84 minutes and the buildup of Rac activity precedes the onset of protrusion by 4.03 minutes on average (Fig 11F). Similarly, we found that the decay of Rho activity precedes the onset of protrusion by on average 5.23 minutes and that the decay of Rac activity typically precedes the onset of retraction, on average by 3.84 minutes (Fig 11F). We did not find the distribution of these buildup and decay lags to be markedly different from each other for a given protein or between the two Rho GTPases (Fig 11F).

Overall, we have shown that Rho activity was elevated in membrane retractions and reduced in membrane protrusions, whereas Rac activity was elevated in protrusions and reduced in retractions. Through cross-correlation analysis of edge velocity and Rho GTPase activity, we have demonstrated that the onset of retraction precedes peak Rho activity, and the onset of protrusion precedes peak Rac activity. However, a closer analysis of edge velocity and Rho GTPase activity in protrusion-retraction cycles has established that the start of Rho activity buildup precedes the onset of retraction, and the start of Rac activity buildup precedes the onset of protrusion.

Our observation that smaller cells are more likely to migrate, while elongated cells are typically unable to do so, led us to hypothesize that this is due to the existence of a threshold distance beyond which Rho GTPase signalling cannot propagate. We thus sought to quantify the spatial propagation of Rho and Rac activity inside the cell during protrusion-retraction cycles. For this, we averaged Rho activity in the entire cell over the cell length for each frame and looked at the top 10% of Rho activity in each cell (Fig 11G). We then visually quantified the approximate amount of the cell length over which we saw spatial propagation of elevated Rho activity to or from the cell edge. Spatial propagation of Rho GTPase activity occurred over up to 45% of the cell length, on average occurring over ~27.5% of cell length for Rho and for ~28% of cell length for Rac (Fig 11H). In microns, this corresponded to an average of ~49 µm for Rho and an average ~34 µm for Rac (Fig 11I), although these distances were found to be correlated to cell length. In terms of spatial propagation relative to cell length, we did not find any notable difference in the amount of spatial propagation between Rho and Rac. While these findings suggest that Rho GTPase signalling is unable to propagate over the entirety of cells with periodic protrusion-retraction cycles, further analysis is required to determine if this limited spatial propagation is the reason for which elongated cells are unable to migrate.

Consistent with data from randomly motile HUVEC acquired by a previous student in the Hayer Lab, we found that Rho activity is higher in membrane retractions and Rac activity is higher in membrane protrusions. This analysis, however, contradicts the findings of Machacek et al., which found Rho activity was elevated early in protrusion, whereas elevated Rac activity appeared with a temporal lag at the protruding cell edge (9). Possible reasons for the discrepancies are differences between cell types and the use of distinct FRET probes. Our analysis of Rho GTPase signalling in cells in periodic protrusion-retractions cycles also revealed that these cycles can be used to study the temporal sequence of edge movement and Rho GTPase signalling events to better understand the driving forces behind membrane protrusions and retractions.

We further showed that the buildup of Rho activity precedes the onset of retraction, and the buildup of Rac activity precedes the onset of protrusion. It remains unclear, however, whether the decay of Rho and Rac activities precede the onset of protrusions and retractions, respectively. Comparing Rho and Rac activities during the transitions between protrusions and retractions in data acquired at higher temporal resolution may provide new insight into the spatiotemporal coordination of Rho GTPase activity during these edge movements. Finally, the restrained range of buildup and decay lags of Rho GTPase activity compared to the broad range of protrusion-retraction cycle durations constitutes evidence of the tight regulation of Rho GTPase activity in time during the transitions between protrusions and retractions.

4.4 Rho Signalling Dynamics Depend on Properties of Retraction in Cells Migrating on Lines of Extracellular Matrix

Previous studies of Rho GTPase signalling dynamics in migrating cells have demonstrated their complexity and precise nature of their spatiotemporal regulation (8,9,55). Despite their key roles as mediators of cytoskeletal reorganization, Rho GTPase signalling dynamics in migrating cells remain incompletely characterized. Using ratio-metric FRET and computational analysis, we aimed to quantify Rho signalling activity in migrating cells. By comparing the Rho GTPase signalling dynamics of autonomously migrating cells to each other and to those of non-migrating cells, we expect to gain a greater understanding of the signalling activities required for cells to migrate. In particular, we sought to determine whether gradients of Rho activity are necessary for cell migration, given reports of its activity both early in membrane protrusion and at the rear of migrating cells (8,9,56).

We found that steadily migrating cells (Fig 12A) had stable retractions at their rear and stable protrusions at their front, where Rho activity was elevated in these stable retractions (Fig 12B) and Rac was elevated in stable protrusions (Fig 12C). However, not all cells migrated smoothly, and many of them stalled often and had transient protrusion and retraction events (Fig 12D). We categorized these cells as "stop-and-go" migrating cells. Interestingly, we observed that Rho activity was higher in these transient retractions compared to stable retractions at the cell rear (Fig 12E).

Because migrating cells with transient retractions at their front would likely have shallower gradients of Rho activity, we sought to determine whether there was a relationship between the steepness of the back-to-front Rho activity gradient and cell displacement. To determine the steepness of the Rho activity gradient in each cell, we created a binary mask of a band around the perimeter of the cell (Fig 12F). For each frame, we averaged Rho activity within the mask along the length of the cell to obtain a vector (Fig 12F). We then averaged these vectors to obtain the Rho activity over time as a function of position along the length of the cell, from top to bottom (Fig 12F). We calculated the steepness of the gradient by fitting a line to the average Rho activity vector and determining the slope of this fit line (Fig 12F).

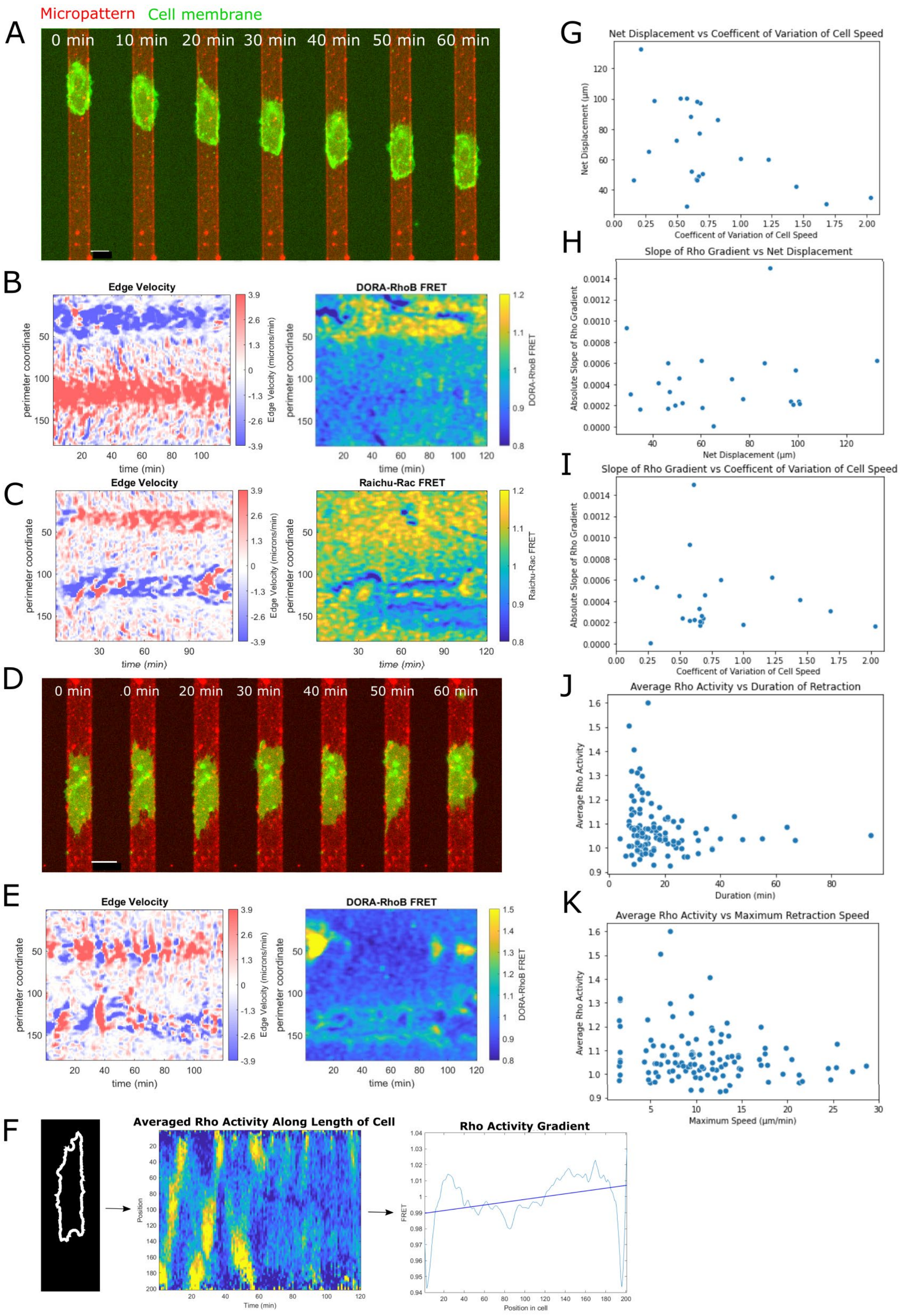
A
Micropattern
Cell membrane
0 min
10 min
20 min
30 min
40 min
50 min
60 min
B
Edge Velocity
DORA-RhoB FRET
perimeter coordinate
time (min)
Edge Velocity (microns/min)
DORA-RhoB FRET
C
Edge Velocity
Raichu-Rac FRET
Raichu-Rac FRET
D
0 min
.0 min
20 min
30 min
40 min
50 min
60 min
E
Edge Velocity
DORA-RhoB FRET
F
Averaged Rho Activity Along Length of Cell
Position
Time (min)
Rho Activity Gradient
FRET
Position in cell
G
Net Displacement vs Coefficent of Variation of Cell Speed
Net Displacement (µm)
Coefficent of Variation of Cell Speed
H
Slope of Rho Gradient vs Net Displacement
Absolute Slope of Rho Gradient
Net Displacement (µm)
I
Slope of Rho Gradient vs Coefficent of Variation of Cell Speed
Absolute Slope of Rho Gradient
Coefficent of Variation of Cell Speed
J
Average Rho Activity vs Duration of Retraction
Average Rho Activity
Duration (min)
K
Average Rho Activity vs Maximum Retraction Speed
Average Rho Activity
Maximum Speed (µm/min)

Figure 12. Rho signalling dynamics depend on properties of retraction in cells migrating on lines of extracellular matrix A, D) HT73 DORA-RhoB cells on micropatterns of ECM proteins, DORA-RhoB used as a membrane marker, AF647-conjugated fibrinogen used to visualize micropatterns. A) Example of cell smoothly migrating on micropatterned line, scale bar = 20 µm, representative of 11 cells from 3 trials. B) Edge velocity and Rho activity maps for cell in A, representative of 11 cells from 3 trials. C) Example edge velocity and Rac activity maps from smoothly migrating cell, representative of 7 cells from 4 trials. D) Example of "stop-and-go" migrating cell, scale bar = 20 µm, representative of 13 cells from 3 trials. E) Edge velocity and Rho activity maps for cell in D. F) Illustration of methodology used to calculate steepness of Rho activity gradient, representative of 13 cells from 3 trials. G) Net displacement as a function of coefficient of variation of cell speed. H) Absolute value of slope of Rho gradient as a function of net displacement. I) Absolute value of slope of Rho gradient as a function of coefficient of variation of cell speed. J) Average Rho activity of retraction as a function of retraction duration. K) Average Rho activity of retraction as a function of maximum speed of retraction. B, C, E) Edge velocity and Rho GTPase activity maps at edge depth of 3 µm. G, H, I) 24 cells from 3 trials. J, K) Rho activity and retraction parameters calculated for edge depth = 3 µm. 115 retractions from 24 cells from 3 trials.

We quantified the smoothness of cell migration by calculating the coefficient of variation of their speeds (CV_{speed}), which represents the standard deviation of cell speed over the mean cell speed. Cells which migrated smoothly thus had a lower CV_{speed}. We found that while net displacement and CV_{speed} were negatively correlated to each other (Fig 12G), demonstrating that more smoothly migrating cells underwent higher net displacement, there was no apparent relationship between net displacement or CV_{speed} and the steepness of the Rho activity gradient (Fig 12H, I).

As mentioned above, transient retractions appeared to have higher Rho activity compared to the stable, long-lived retractions at the rear of migrating cells. To determine which properties of retractions were most closely related to their average Rho activity, we first compared their average activity to their duration. Consistent with our observations, we found that longer-lived retractions had relatively low levels of Rho activity and the retractions with the highest Rho activity were short-lived, lasting between approximately 10-20 minutes (Fig 12J). We also characterized the relationship between the maximum speed of a retraction and its average Rho activity. The relationship between these two parameters was less clear, with the fastest retractions generally having relatively low Rho activity and retractions with the highest average Rho activities having maximum speeds between 0 and 15 µm/min (Fig 12K).

Overall, the signalling dynamics of migrating and non-migrating cells were found to be significantly different. Cells with periodic protrusion-retraction cycles had oscillatory Rho GTPase activities, whereas signalling activities in migrating cells were more stable. Investigating the Rho GTPase activities of migrating cells revealed that the steepness of the Rho gradient does not predict how effectively a cell will migrate, with many migrating cells having shallow gradients of activity. In contrast to the textbook view, which dictates that all migrating cells have a back-to-front gradient of Rho activity, these results suggest that pronounced gradients of Rho activity are not necessary for cell migration. However, investigating the relationship between retraction duration and average Rho activity revealed that long-lived retractions have relatively low Rho activity, while the retractions with the highest Rho activity are transient. This finding is consistent with Rho activity being self-limiting due to slow negative feedback, as is characteristic of excitable systems (11). Unfortunately, it was difficult to obtain a sufficient number of migrating cells expressing Raichu-Rac, as the necessary use of a higher-magnification objective lens (40x for Raichu-Rac compared to 20x for DORA-RhoB) resulted in a smaller field of view while imaging. The use of this objective was required due to the lower expression and/or fluorescence intensity of Raichu-Rac relative to DORA-RhoB. As such, further experiments will need to be conducted to perform a similar analyses of Rac activity gradients in autonomously migrating cells, as well as an analysis of the relationship between Rac activity and protrusion parameters. Such analyses would allow us to determine the ways in which Rho and Rac signalling differ in autonomously migrating cells.

4.5 Pattern Area Impacts Cell Motile Behavior on Micropatterned Circles of Extracellular Matrix

Given our finding that cell shape impacts the likelihood of a cell undergoing directed migration on micropatterned lines, we further sought to determine whether micropattern size and cell motile behaviour were linked for cells adhering on micropatterned circles, where they were forced into a non-polarized morphology. To do this, we imaged single cells plated on micropatterned circles of 20-70 μm in diameter. Only single cells on micropatterns which covered over 90% of the pattern area over the course of imaging were considered. Interestingly, irrespective of pattern size, a number of cells plated on these micropatterned circles exhibited some form of protrusive activity. We visually classified cells into groups based on their protrusive activities, which included membrane blebs (Fig 13A), lamellipodia (Fig 13B) and thin, longer lived membrane protrusions (Fig 13C) which we refer to as “small protrusions”. The remaining population of cells, the majority of which had membrane ruffling activities along the edge of the micropattern, were categorized as “other”. We found that within the 30-minute imaging time, the majority of cells plated on 20 µm-diameter circles and approximately one quarter of those plated on 30 µm circles had membrane blebs (Fig 13D). A number of cells plated on 40-70 µm-diameter patterns had sheet-like, lamellipodial protrusions (Fig 13D). The proportion of cells which had these sheet-like protrusions increased with micropattern diameter. Finally, “small protrusions” were observed on micropatterns of all sizes, where 50 µm circles had the largest proportion of cells exhibiting this activity. (Fig 13D).

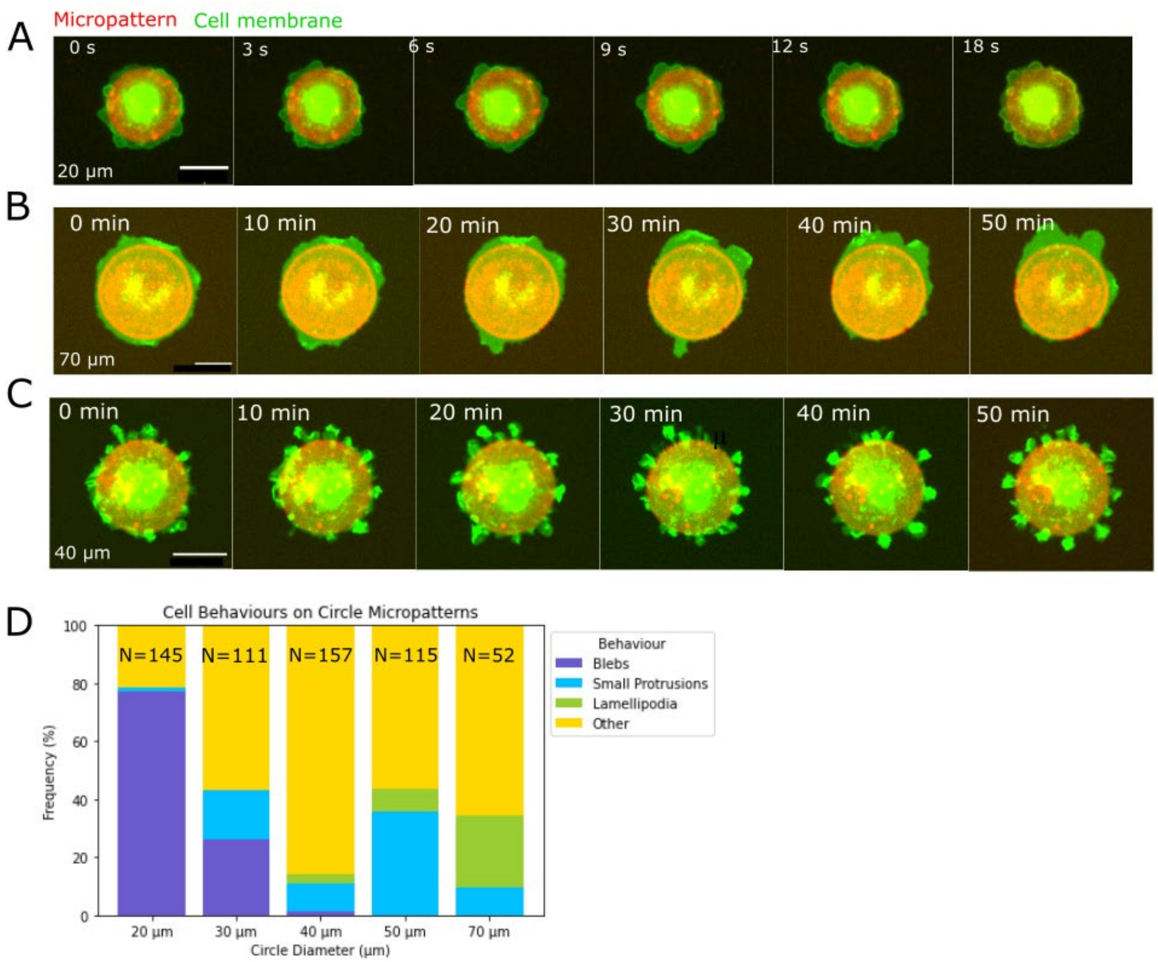

Figure 13. Cells plated on micropatterned circles exhibit different types of protrusive activities. HT73 DORA-RhoB HUVEC were seeded onto coverslips with micropatterns of fibronectin and AF-647 conjugated fibrinogen. Cells on 20 µm, 30 µm, 40 µm, 50 µm and 70 µm micropatterned circles were imaged at 25-second intervals for 30 minutes. A) Blebbing cell on 20 µm-wide circle. Scale bar = 20 µm. B) Cell with sheet-like lamellipodial protrusions on 70 µm-wide circle. Scale bar = 30 µm. C) Cell with “small protrusions” on 40 µm-wide circle. Scale bar = 30 µm.d) Quantification of cell motile behaviours as a function of micropattern diameter. 580 cells from 3 trials.

Unexpectedly, we found that despite imposing a non-polarized shape on cells, they often exhibited different dynamic protrusive activities with timescales ranging from seconds for blebs to tens of minutes for lamellipodia and "small protrusions". Our results highlight the ways in which 2D confinement impacts cell motile behaviour, while additionally providing a tool for the investigation of certain behaviours which can be generated on micropatterns of different widths. 20 μm-diameter micropatterned circles can be used to reproducibly generate blebbing cells. The activities of different proteins in cells with transient membrane blebs can be investigated using cells plated on these micropatterns. We have also observed that cells plated on 50-70 μm circles, which occupy around 70% of the micropattern area, can be used to investigate signalling activity in cells with sheet-like membrane protrusions and retractions while avoiding extended branch-like cellular processes which might complicate downstream computational analysis.

4.6 Front-Back Gradients of Rho and Rac Activity Have Different Relationships to Net Displacement in Collectively Migrating Cells

The major difference between collective cell migration and autonomous cell migration is that collectively migrating cells interact with their neighbours, and these interactions are known to alter their migration (1,21). As discussed in an earlier section, collective cell migration is often more effective than autonomous migration on uniform substrates because collectively migrating cells move with higher directional persistence (21). In endothelial cells, cadherin fingers, which extend from leader cells to follower cells, might influence the polarity of the follower cells, thus impacting their migration (22). The confinement of cryptic lamellipodia under neighbouring cells has also been found to promote more stable actin structures which extend at higher speeds (74). The presence of cryptic lamellipodia might also contribute to persistence by preventing cells from stalling or slipping backwards (74). Given these cell-cell interactions likely lead to differential cytoskeletal dynamics in collectively migrating cells, comparing the signalling dynamics of cells migrating autonomously and collectively may lead to new insight on the signalling networks that control cell migration.

To investigate the signalling dynamics of collectively migrating HUVECs, we created mosaic monolayers by seeding a mix of either DORA-RhoB or Raichu-Rac expressing cells with fluorescently tagged VE-cadherin (CDH5-mRuby3) expressing cells (Fig 14A, C, D), allowing us to visualize cell-cell junctions in the monolayer while studying Rho GTPase signalling.

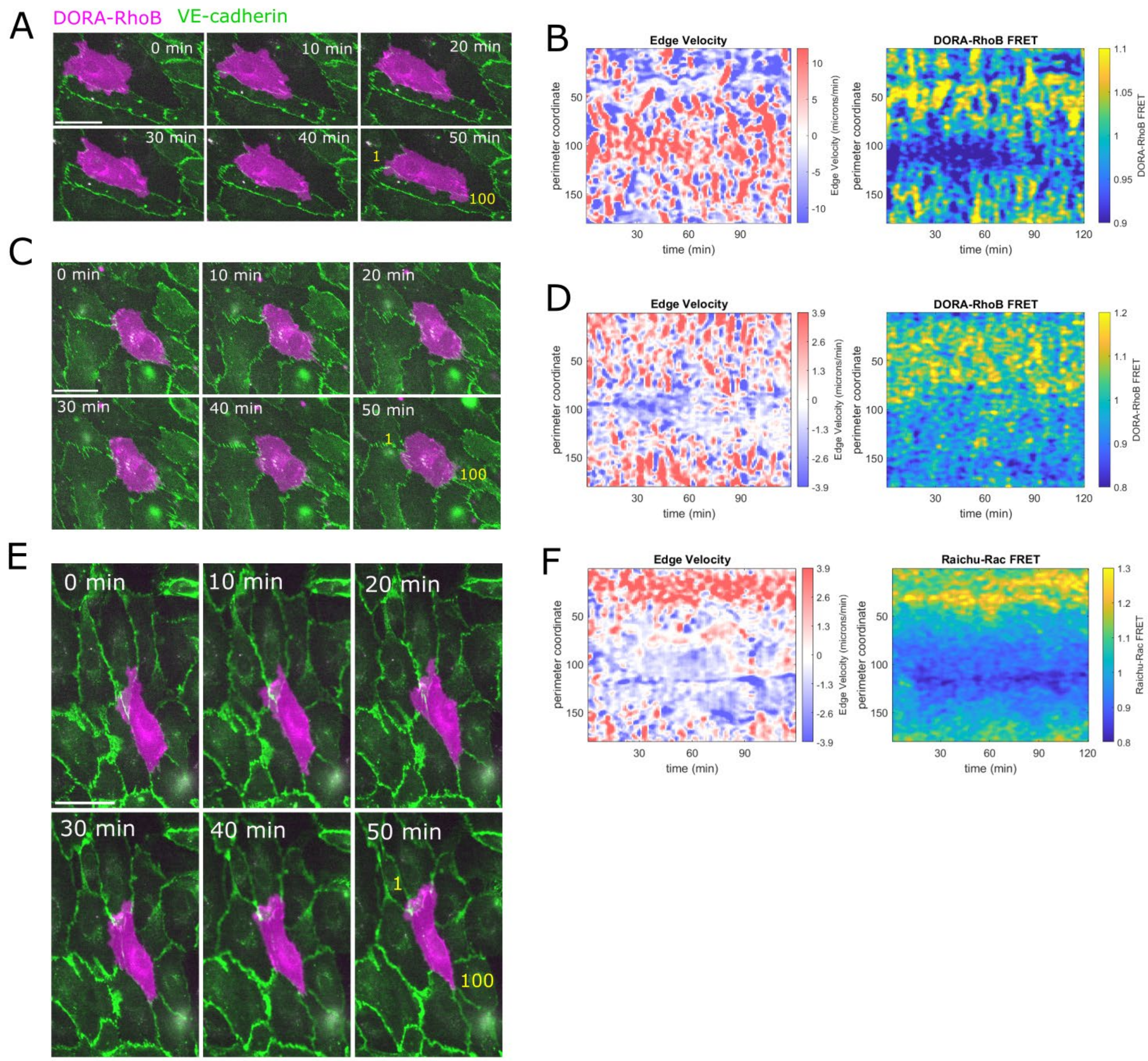

Figure 14. Examples of Rho GTPase signalling in collectively migrating cells. A, C) Examples of collectively migrating HT73 DORA-RhoB cells in a mosaic monolayer with VE-cadherin-mRuby3 expressing cells, scale bar = 50 µm. B) Edge velocity and Rho activity map for A. D) Edge velocity and Rho activity map for A. E) Example of collective migrating HT73 Raichu-Rac cells in a mosaic monolayer with VE-cadherin-mRuby3 expressing cells. F) Edge velocity and Rac activity maps for cell in E, scale bar = 50 µm. A, C, E) Numbers in yellow indicate perimeter coordinates (labelled starting from top left, clockwise) B, D, F) Edge velocity and Rho GTPase activity maps at edge depth of 3 µm.

HUVECs, which collectively migrate *in vivo* during angiogenesis, undergo spontaneous collective migration when plated in monolayers on uniform 2D substrates, whereas when plated individually on 2D substrates, they typically fail to both polarize and migrate, instead displaying local membrane protrusion and retraction cycles. While, as previously described, we were able to observe HUVECs migrate autonomously on micropatterned lines, these cells were restricted in their interactions with neighbouring cells and in the range of morphologies they can adopt. In contrast, cells collectively migrating in monolayers are able to turn varying degrees, can mechanically interact with their neighbours and are confined by them by varying amounts (15,21). However, the added complexity of this context might make it more difficult to determine the extent to which different parameters contribute to the observed behaviours and signalling dynamics.

As with cells migrating on micropatterned lines, we observed that collectively migrating cells could have gradients of Rho activity, where Rho was higher at the cell rear (Fig 14A, B), but that this was not always the case (Fig 14C, D). However, our observation suggested that most if not all migrating cells had visible gradients of Rac activity, with elevated activity at the leading edge of the cell (Fig 14E, F). Consistent with our findings from cells migrating on micropatterned lines, we found that Rho activity was elevated in retractions and reduced in protrusions, and that there is a significant difference in Rho activity at the cell edge in these two behaviours (Fig 15A). Cross-correlating cell edge velocity and Rho activity once again showed the negative correlation between edge velocity and Rho activity. It additionally revealed a temporal lag of 1 minute between edge velocity and Rho activity (Fig 15B). As expected, Rac activity was elevated in protrusions and reduced in retractions (Fig 15C). In this case edge velocity and Rac activity were positively correlated, with a temporal lag of 1 minute between the two (Fig 15D).

To determine if our findings in cells on micropatterned lines could be replicated in collectively migrating cells, we examined the relationship between Rho activity and both retraction duration and the maximum speed of retraction (Fig 15E, F). We found again that longer-lived retractions have relatively low Rho activity, however the duration of retractions with the highest Rho activity were heterogeneous in collectively migrating cells (Fig 15E). We also quantified the relationships between Rac activity and protrusion duration and Rac activity and maximum speed (Fig 15 G, H). We did not find any significant relationships between these parameters.

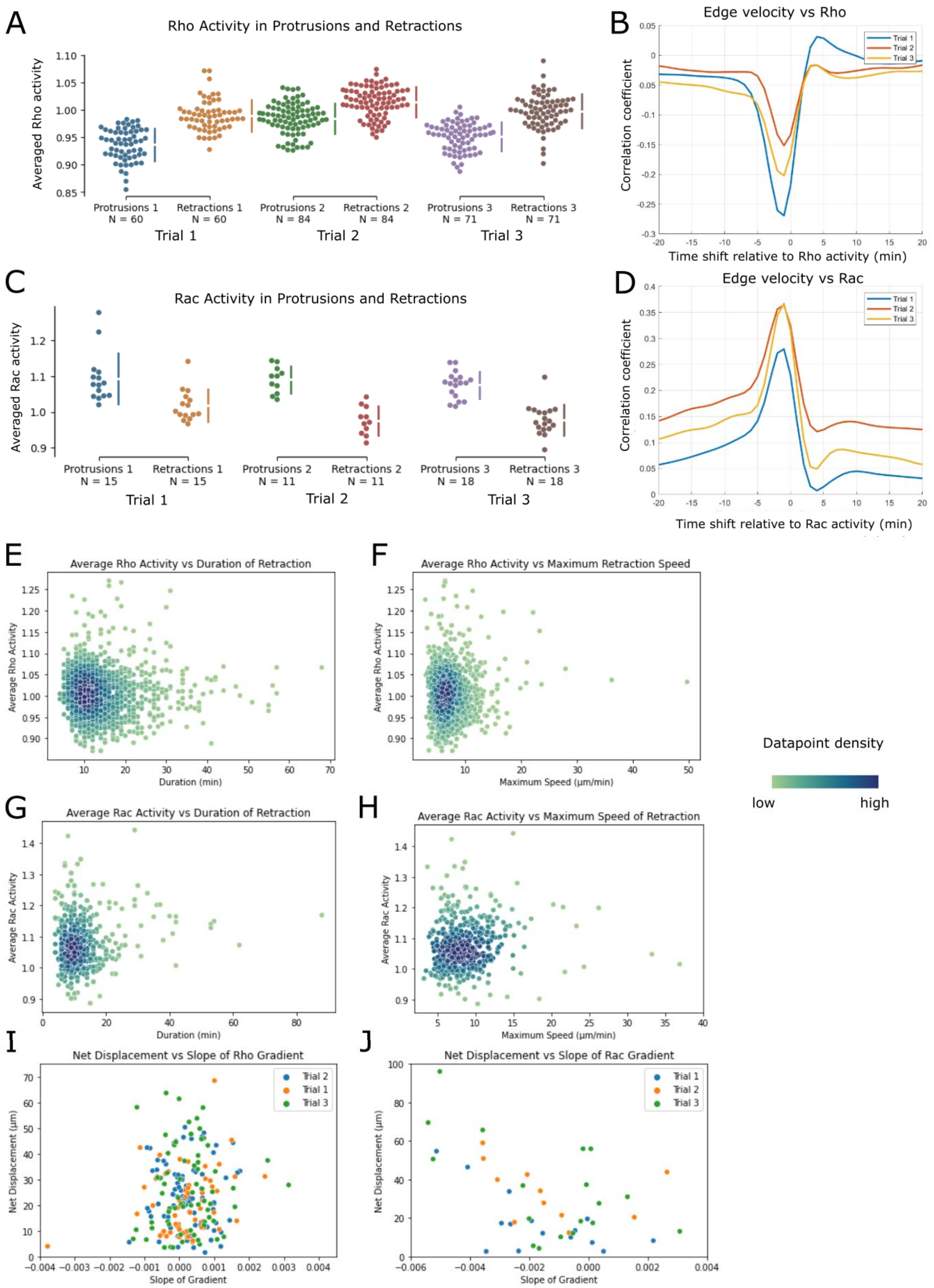

Figure 15. Rho and Rac signalling patterns differ in collectively migrating cells. A) Rho activity in cell edge

protrusions and retractions. P-values from Mann-Whitney: 1.88e-17 (trial 1), 7.62e-10 (trial 2), 9.15e-10 (trial 3). B) Cross-correlation of edge velocity and Rho activity, peak temporal lag of -1 minute. C) Rho activity in protrusions and retractions of the cell. P-values from Mann-Whitney: 4.94e-4 (trial 1), 1.07e-4 (trial 2), 3e-6 (trial 3). D) Cross-correlation of edge velocity and Rac activity, peak temporal lag of -1 minute. E) Rho activity as a function of retraction duration. F) Rho activity as a function of maximum speed of retraction. G) Rac activity as a function of protrusion duration. H) Rac activity as a function of maximum speed of protrusion. I) Net displacement as a function of Rho gradient slope. Positive slope values indicate elevated Rho activity at the cell rear compared to the cell front. J) Net displacement as a function of Rac gradient slope. Negative slope values indicate elevated Rac activity at the cell front compared to the cell rear. A, B, E, I) 215 cells from 3 trials. C, D, G, H, K) 44 cells from 3 trials. G, H) Three retractions with speeds>100 µm/min were excluded, as these speeds were likely due to an analysis error.

To visualize the relationship between gradients of Rho GTPase activity and migration, we calculated the slope of front-back Rho and Rac activity gradients and compared the steepness of these gradients to the corresponding cell's net displacement. Using custom code, the steepness of GTPase activity gradients was calculated such that if activity was higher at the front, the slope of the gradient would be negative and, conversely, if it was higher at the rear the slope of the gradient would be positive. While we were unable to observe any clear relationship between net displacement and the steepness of front-back Rho gradients (Fig 15I), we noticed that cells with steeper Rac gradients tended to migrate further (Fig 15J).

These differences in the relationships between the slope of Rho and Rac gradients in cells and their net displacements suggest that a steep back-to-front Rho gradient might not be a requirement for migration. Cells that migrated the furthest seem to have relatively shallow Rho activity gradients, if any. Combined with our finding that the retractions with the highest average Rho activity tend to be short-lived, this suggests that the long-lived stable retractions at the rear of migrating cells do not require Rho activity to be highly elevated for the entire time the cell is migrating. Another difference between Rho and Rac activity is illustrated by the cross-correlation analysis with edge velocity. While the correlation coefficients between edge velocity and Rho were similar to those for edge velocity and Rac in cells with periodic protrusion-retraction cycles, here edge velocity and Rac seem to be more strongly correlated than edge velocity and Rho. A major difference between the types of retractions in these two settings is that some of the retractions in collectively migrating cells are long-lived, whereas this is not the case for cells with protrusion-retraction cycles.

4.7 Cell Shape Is Not Sufficient to Predict Migratory Phenotype of Collectively Migrating Cells

Given that we observed a relationship between cell shape and cell motile behaviour for cells plated on micropatterned lines, we next compared cell shape to cell motile behaviours for cells migrating in monolayers. To do this, we calculated cell motility parameters based on movement of the centroid of segmented cells expressing DORA-RhoB from the previous section. The parameters used in our analysis were net displacement, persistence, and average velocity, where persistence is defined as the ratio of net displacement to total displacement. We additionally normalized net displacement to cell length, providing a metric for displacement relative to cell body length. Further, we obtained morphological information for cells using VAMPIRE, as was done for cells on micropatterned lines. Our morphological parameters of interest were cell area, cell length and cell aspect ratio.

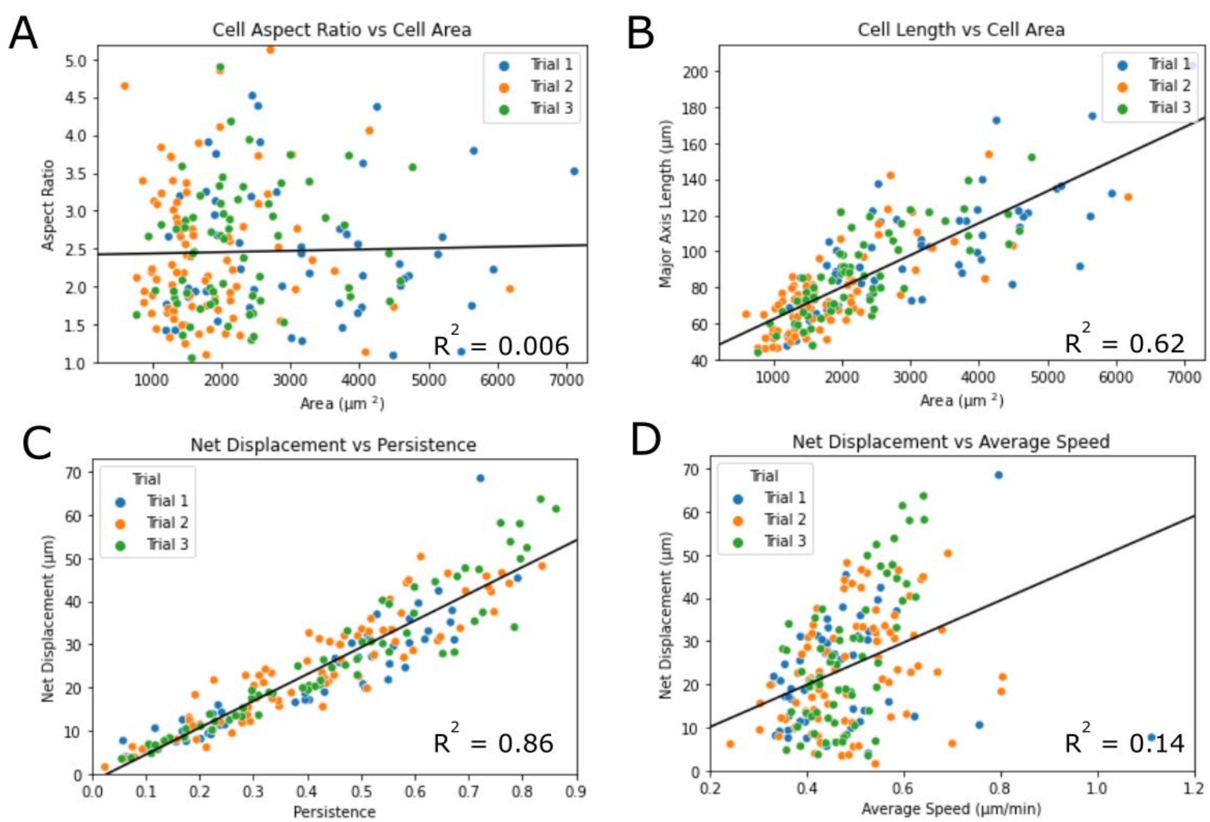

Figure 16. Analysis of morphology and motility for cells plated on micropatterned lines. A) Cell aspect ratio as a function of cell area. B) Cell length as a function of cell area. C) Net Displacement as a function of persistence. D) Net displacement as a function of average velocity. A-D) 203 cells from 3 trials. Fit lines (in black) calculated using linear regression. Each dot represents one cell.

Morphological analysis of these cells revealed that cells with a larger area tended to be longer (Fig 16B), however cells of all areas had a similar range of aspect ratios (Fig 16A), demonstrating that these cells tend to adopt a consistent range of shapes independent of their areas. Analysis of cell motility parameters revealed that persistence and net displacement were clearly correlated, as was expected (Fig 16C).

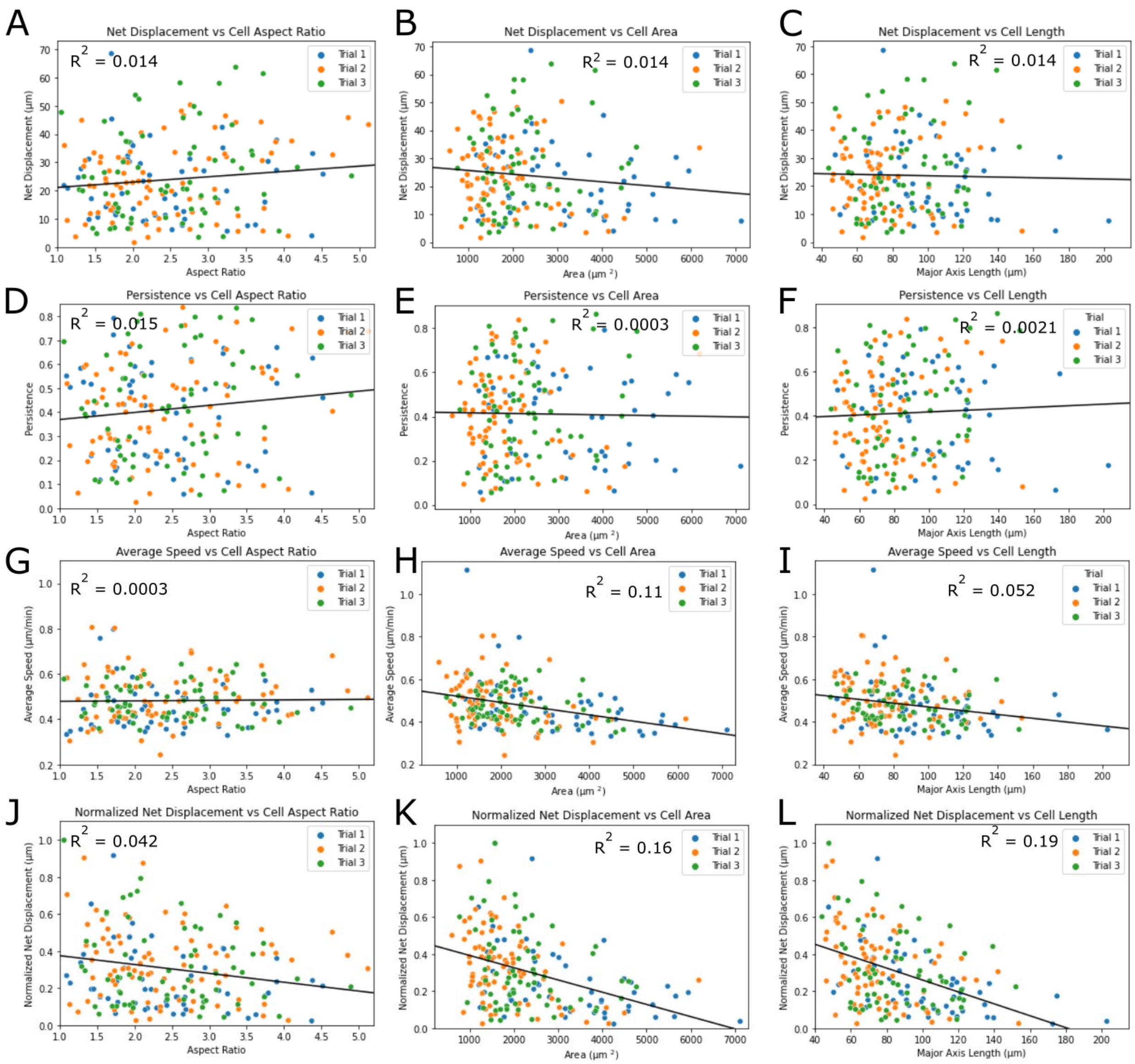

Figure 17. Cell shape is not sufficient to predict migratory phenotype of collectively migrating cells. Net displacement as a function of A) Cell aspect ratio B) Cell Area C) Cell length. Directional persistence of migration as a function of D) Cell aspect ratio E) Cell Area F) Cell length. Average speed as a function of G) Cell aspect ratio H) Cell Area I) Cell length. Net displacement normalized to cell length as a function of J) Cell aspect ratio K) Cell Area L) Cell length. A-L) 203 cells from 3 trials. Fit lines (in black) calculated using linear regression. Each dot represents one cell.

To examine the relationship between cell shape and cell motility in collectively migrating cells, we combined our analysis of cell morphology with our analysis of cell motility. We compared net displacement, persistence and average velocity to cell area, cell length and cell aspect ratio. These analyses revealed that the variables with the strongest correlations or anticorrelations are average velocity and cell area (Fig 17H), normalized net displacement and cell length (Fig 17K), as well as normalized net displacement and cell area (Fig 17L). However, there is no case in which there exists a clear linear relationship between a shape parameter and a motility parameter. The data suggests that longer and larger cells do not attain high speeds, and that relative to their length, these cells undergo less displacement. Shorter or smaller cells, though, appear able to adopt a wider range of migratory phenotypes, displaying more variation in average velocities and displacement relative to cell length. This discrepancy might be due to the potential influence of cell's neighbours' migration velocities on its own velocity. A cell might be slowed down by a slow neighbour or pulled along by a fast-moving neighbour.

5 DISCUSSION

With this project, we aimed to gain a greater understanding of the differences between autonomous and collective cell migration, as well as how cell shape affects cell migration behavior and Rho GTPase signaling dynamics. Based on the observation that sparsely plated HUVECs on uniform 2D substrates typically adopt a multipolar morphology and do not migrate, while HUVECs plated in monolayers undergo spontaneous collective migration, we first aimed to determine if the morphologies of cells plated on micropatterned lines were related to their motile behaviours. We characterized the spatiotemporal signalling dynamics of the Rho GTPases Rho and Rac in migrating and non-migrating cells, with the goal of understanding how they might differ between the two scenarios. Then, we characterized the Rho GTPase signalling activities of cells in monolayers, and we examined the relationship between cell shape and cell motile behaviour for these cells. We compared our findings from cells on micropatterned lines to those from collectively migrating cells to elucidate whether the relationships between motility and morphology remained the same, as well as to investigate whether Rho GTPase signalling activities observed in autonomously migrating cells were altered in collectively migrating cells.

Overall, we found that different behaviours of interest can be observed in cells plated on micropatterned lines and circles. We showed that HUVECs with larger adhesion surfaces that are more elongated in shape than what is typically found in cell monolayers, are unable to migrate significant distances autonomously. Additionally, we discovered possible key differences between the signalling dynamics of Rho and Rac, namely regarding the importance of gradients of their activities for directed cell migration, and the relationship between their activities and the duration of the protrusion or retraction they are associated with.

First, we quantified cell motile behaviours on micropatterns of ECM proteins, which revealed that a number of behaviours can reliably be generated with this technique. On micropatterned lines, we were able to observe autonomously migrating cells, as well as non-migrating cells, many of which had periodic protrusion-retraction cycles at their competing fronts. Several previous studies have used asymmetric micropatterns to generate migrating cells (72,73), or have used micropatterned lines to observe collectively migrating cells (84). We used micropatterned lines to generate autonomously migrating HUVECs, which typically do not migrate when plated sparsely on a uniform substrate. This allowed us to perform a more in-depth quantitative analysis of morphology and Rho GTPase signalling in these cells. In addition, we are, to our knowledge, the first to report generating cells with periodic protrusion-retraction cycles using micropatterned lines. These repetitive cycles of edge movement have proven to be a valuable tool for quantifying Rho GTPase activity in protrusions and retractions, as well as for characterizing the relationship between Rho GTPase activity and edge velocity in individual protrusion-retraction cycles.

Comparing the morphology and motility of cells plated on micropatterned lines showed that smaller, shorter, less elongated cells are more likely to migrate, and that these cells are most often found on 20 μm-wide micropatterned lines. Thus, the odds of observing migrating cells can be increased by searching for and imaging fields of view containing smaller, shorter, less elongated cells. To further increase the frequency of observed migration events, it might be useful to sort cells by size using Fluorescence-Activated Cell Sorting (FACS). Plating the smallest 20% of the cell population on 20 μm-wide micropatterned lines should result in over half of the cells migrating. This would be particularly useful when imaging with higher magnification objectives, such as a 40x or 60x, and while using probes which are not very well expressed by cells.

While our findings on the relationship between morphology and motility in cells plated on micropatterned lines might initially seem counterintuitive given that cells that have undergone epithelial-mesenchymal transition (EMT) are more elongated and more migratory (85). However, based on the quantification of the elongation ratio (which is calculated similarly to aspect ratio) of HMEC-1 cells during endothelial-mesenchymal transition (EndMT) by Ciszweski et al. (86), both control cells and cells treated with TGFβ had elongation ratios similar to those of the "smallest" cells on 20 um micropatterned lines in our experiments, thus the scale of the change in morphology in these two scenarios is different, and not particularly suitable for comparison. It is also important to note that during EMT, cells transition from both less to more migratory and from stronger to weaker cell-cell adhesion, whereas in our experiments, cell-cell adhesion was not involved.

Besides studying motility of cells plated on micropatterned lines of ECM, we also investigated motility phenotypes on micropatterned ECM circles, as a function of circle diameter. For example, 20 μm-diameter circles are ideal for generating blebbing cells and can be used to quantify protein activity within these blebs. Few studies have investigated Rho signalling in these blebs (87,88), and the anillin-based localization probe used for this purpose might be slow to capture the signalling dynamics of such a rapid process, which occurs on the order of seconds. Preliminary data from our work with the DORA-RhoB probe has shown Rho activity to spike during bleb protrusion, not retraction as was shown by Aoki et al.(87), though additional experiments are required to determine the reason for these discrepancies in timing.

We characterized the Rho GTPase signalling dynamics of migrating and non-migrating cells on micropatterned lines using FRET and computational analysis. Cells with periodic cycles of membrane protrusions and membrane retractions had oscillatory Rho and Rac signalling dynamics, which we quantified. Like Machacek et al. and Martin et al., we used cell edge movement events such as the onset of protrusion and retraction as reference points, and compared the Rho GTPase signalling activities of different cells to each other with respect to these events (9,56). We found that there was significantly higher Rho activity in retractions than in protrusions, and significantly higher Rac activity in protrusions than in retractions. Further, the onset of protrusion and retraction preceded peak Rac and Rho activity, respectively. While our current findings regarding Rho activity in protrusions and retractions differ from Machacek et al., who found elevated Rho activity early in protrusions, we also found that peak Rac activity does not drive the initiation of membrane protrusions (9). Our findings on Rho activity in protrusions are more closely aligned to those by Yang et al., who found protrusions to have reduced RhoA activity (8).

Ambiguity on the ordering of Rho GTPase signalling events during the transitions between protrusions and retractions remains. Further analysis of protrusion-retraction cycles, ideally in cells that express FRET probes for both Rho and Rac, could provide clarity on the sequence of Rho GTPase signalling events during these transitions. Because of the antagonism between Rho and Rac activities, a reduction in the level of one protein would likely result in an increase in the activity of the other and vice-versa (6,11).

Taking our results on the relationship between cell morphology and cell motile behaviour together with our characterization of Rho GTPase signalling in cells with protrusion-retraction cycles, we attempted to explain why larger, longer cells with highly elongated shapes are unable to migrate. We hypothesized that there exists a threshold distance beyond which Rho GTPase activity cannot propagate. This would lead to a failure of the cell front and cell rear to coordinate their activities and would explain why, although we see sizable protrusions and retractions in cells with periodic protrusion-retraction cycles, these cells remain unable to polarize. This hypothesis would be consistent with a study by Bolado-Carrancio et al., where the authors suggested that travelling waves of Rho and Rac activity coordinated the front and rear of migrating breast cancer cells (58). Thus, if these coordinating waves of activity were unable to propagate from the cell front to the cell rear due to the high degree of elongation imposed by micropatterned lines, it would result in a lack of coordination between the leading and trailing edges, which could manifest as competing cell fronts. Our quantification of the spatial propagation of Rho GTPase activity in cells with protrusion-retraction cycles found that elevated Rho and Rac activity could propagate over at most 45% of cell length. As such, in cells with periodic protrusion-retraction cycles, Rho GTPase activity does not appear to be able to propagate over the entire length of the cell.

We again used ratio-metric FRET and computational analysis to investigate the Rho GTPase signalling dynamics of autonomously migrating cells. Comparing the net displacement of these migrating cells to the steepness of their Rho gradient, we found no discernable relationship between the two. However, calculating an average Rho activity gradient over time might obscure transient or very shallow gradients. It would therefore be pertinent to conduct a more in-depth analysis of Rho activity and cell movement, by comparing the Rho gradient in individual frames with cell displacement between the current frame and the subsequent frame.

In autonomously migrating cells, analysis of Rho activity in retractions revealed that average activity was linked to the duration of retraction, and that retractions with the highest activity were transient. This suggests that Rho activity might be self-limiting, with fast buildup of activity through positive feedback and slower negative feedback, as is often found in excitable signalling networks (11). Excitable signalling networks involving Rho activity have previously been described, including one proposed by Graessl et al. to control subcellular contractions, with fast amplification of Rho activity through GEF-H1 and slow inhibition through Myo9b (12). The relatively limited range of Rho GTPase buildup and decay lag durations in comparison to the range of protrusion-retraction cycle durations in cells with periodic protrusion-retraction cycles further supports that Rho GTPase activities are tightly regulated, likely through positive and negative feedback loops.

Future work in migrating cells will involve determining whether the activities of actin and myosin are different in transient protrusions and retractions, and whether these differences or lack of differences are related to different Rho GTPase signalling activities. To do this for Rho activity, we have already created a cell line, HT73 DORA-RhoB Ftractin-mRuby3 miRFP680-MYL9, where the activities of Rho, actin and myosin can simultaneously be measured in the same cell. Using this cell line and a similar computational and edge velocity analysis we have conducted for Rho GTPases might lead to insight on these observed differences. We can also employ techniques such as Spatiotemporal Image Correlation Spectroscopy (STICS) or Particle Image Velocimetry (PIV) to quantify actin and myosin flow during protrusions and retractions and to investigate their relationship to Rho GTPase signalling dynamics.

To the best of our knowledge, the highly elongated morphology of cells on micropatterned lines, with cells displaying periodic protrusion-retraction cycles, has not yet been linked to migration-related disease phenotypes. However, it might be interesting to investigate how individually migrating cancer cells are able to maintain a shape that favours migration and the invasion of new tissues, or the effects of such a highly elongated morphology on a process such as wound healing. Further, it might be interesting to study Rho GTPase signalling and cell motile behaviour in cells which adopt shapes more similar to those of cells before and after EMT, to determine whether a similar relationship between morphology and migration is observed.

We additionally characterized the Rho GTPase signalling activities of cells collectively migrating in monolayers, employing similar methodology as for cells plated on micropatterned lines. We found that the steepness of the Rho gradient was not clearly related to the net displacement of collectively migrating cells. However, cells with steeper Rac gradients tended to migrate further than those with shallow gradients. This suggests that the presence of a front-to-back Rac gradient is more important for cell migration than the presence of a back-to-front Rho gradient. This difference in the impact of Rho and Rac gradients might be due to differences in their stability or steepness. Experiments using Raichu-Rac expressing HUVECs migrating on micropatterned lines could prove useful, as collectively migrating cells might engage in behaviours such as turning, which could impact their net displacement relative to cells migrating in straight lines while not significantly changing their gradient of Rac activity.

Examining the relationship between Rho activity and retraction duration revealed a more limited relationship in collectively migrating cells than in autonomously migrating cells, and no clear relationship was established between Rac activity and protrusion duration. Additional experiments on Rac activity in transient and long-lived retractions in cells migrating on micropatterned lines might be able to more clearly elucidate how the relationships between Rho and Rac activity and the properties of retractions and protrusions, respectively, differ. Given that the relationship between Rho activity and retraction duration was mostly clearly visible in cells migrating on micropatterned lines, a similar analysis on Raichu-Rac expressing cells would likely lead to more conclusive results.

In comparing the morphologies of cells plated on micropatterned lines to those of collectively migrating cells, we noticed that collectively migrating cells had a much smaller range of aspect ratios and that aspect ratio was not strongly related to net displacement, average cell speed, persistence or net displacement normalized to cell length. In contrast, longer and larger cells, with higher aspect ratios, migrate lesser distances on micropatterned lines. The smaller range of recorded aspect ratios of collectively migrating cells is likely due to geometric restrictions imposed by neighbouring cells and might contribute to an increased proportion of collectively migrating cells. It is possible that if a cell in a monolayer adopted a highly elongated shape, it would undergo far less displacement. However, this potential inability to migrate as efficiently as a cell with a rounder shape would be a functional disadvantage and might explain why HUVECs typically do not appear to adopt this shape in monolayers. We also noted that the relationships between net displacement and both cell area and cell length are weaker in collectively migrating cells compared to cells on micropatterned lines. Since the range of cell lengths and cell areas are once again smaller for collectively migrating cells, the reason for these weaker relationships between cell morphology and cell motility likely follows the same logic as for aspect ratio.

While the strength of the relationships between cell morphology and cell motility differs between autonomously migrating and collectively migrating cells, their Rho GTPase signalling dynamics seem more consistent. For both collectively migrating cells and cells migrating on micropatterned lines, the steepness of the Rho activity gradient does not appear to be linked to its net displacement. Furthermore, cells which migrate on lines in a “stop-and-go” manner often have transient retractions at their front and rear which would interfere with any necessary gradient, but these cells nonetheless undergo substantial net displacement. Although slowdowns due to transient protrusions and retractions might argue for the importance of a stable Rho gradient, certain cells observed also had protrusion-retraction cycles at their front, leading to frequent transient retractions and elevated Rho activity at the cell front, while migrating at a steady pace.

The reason for which the relationship between retraction properties and Rho activity changes slightly in collectively migrating cells is not known. One potential explanation is that the group of more transient retractions recorded in collectively migrating cells corresponds mostly to Junction Associated Intermittent Lamellipodia (JAILs), which might be longer-lived than transient retractions in cells autonomously migrating on micropatterned lines. Confinement of these lamellipodia under neighbouring cells could then stabilize them in a manner similar to the stabilization of cryptic lamellipodia by neighbouring cells (74), thus extending the duration of their retraction. Further, changes in Rac activity based on whether a protrusion came into contact with another cell or not have been documented (55).

6 CONCLUSION

In summary, we have used micropatterned lines of ECM proteins to reproducibly generate autonomously migrating HUVECs, and HUVECs with periodic protrusion-retraction cycles at their competing fronts. Using cells plated on micropatterned lines, we have shown that cell morphology and cell motile behaviour are linked. Large and highly elongated cells on micropatterned lines typically do not migrate, and cells on micropatterned circles exhibit different types of protrusive activities depending on the area of their adhesive surface. Employing a combination of ratio-metric FRET and computational analysis, we have studied the Rho GTPase signalling dynamics of non-migrating, autonomously migrating and collectively migrating endothelial cells. We have demonstrated that the retractions with the highest levels of Rho activity are transient and that long-lived retractions have relatively low Rho activity. Additionally, we have found potential differences in the requirement for gradients of Rho and Rac activity in collectively migrating cells.

We have accomplished our goal of gaining a greater understanding of the differences between autonomous and collective cell migration, specifically in terms of how cell morphology affects cell motile behaviour and how cell-cell interactions might modify the Rho GTPase signalling observed in autonomously migrating cells. In addition to this, we have established that several behaviours of interest can be studied using micropatterns. In the future, it will be interesting to gain additional insight into the reason for which cells with highly elongated morphologies are unable to migrate and to clarify the timing of edge movement events and Rho GTPase signalling events in the transitions between membrane protrusion and retraction.

7 REFERENCES

1. Friedl P, Gilmour D. Collective cell migration in morphogenesis, regeneration and cancer. Nat Rev Mol Cell Biol. 2009;10(7):445–57.

2. SenGupta S, Parent CA, Bear JE. The principles of directed cell migration. Nat Rev Mol Cell Biol [Internet]. 2021 May 14 [cited 2021 May 16];1–19. Available from: http://www.nature.com/articles/s41580-021-00366-6

3. Ladoux B, Mège RM. Mechanobiology of collective cell behaviours. Nat Rev Mol Cell Biol 2017 1812 [Internet]. 2017 Nov 8 [cited 2022 Mar 6];18(12):743–57. Available from: https://www.nature.com/articles/nrm.2017.98

4. Ladoux B, Mège RM, Trepat X. Front–Rear Polarization by Mechanical Cues: From Single Cells to Tissues. Trends Cell Biol. 2016 Jun 1;26(6):420–33.

5. Ridley AJ, Schwartz MA, Burridge K, Firtel RA, Ginsberg MH, Borisy G, et al. Cell Migration: Integrating Signals from Front to Back. Science (80-). 2003;302(5651):1704–9.

6. Lawson CD, Ridley AJ. Rho GTPase signaling complexes in cell migration and invasion. J Cell Biol [Internet]. 2018 Feb 5 [cited 2022 Mar 6];217(2):447–57. Available from: https://doi.org/10.1083/jcb.201612069

7. Hodge RG, Ridley AJ. Regulating Rho GTPases and their regulators. Nat Rev Mol Cell Biol 2016 178. 2016 Jun;17(8):496–510.

8. Yang HW, Collins SR, Meyer T. Locally excitable Cdc42 signals steer cells during chemotaxis. Nat Cell Biol [Internet]. 2016 Jan 28 [cited 2021 Feb 24];18(2):191–201. Available from: https://www.nature.com/articles/ncb3292

9. MacHacek M, Hodgson L, Welch C, Elliott H, Pertz O, Nalbant P, et al. Coordination of Rho GTPase activities during cell protrusion. Nature [Internet]. 2009 Sep 3 [cited 2021 Feb 24];461(7260):99–103. Available from: https://www.nature.com/articles/nature08242

10. Pertz O. Spatio-temporal Rho GTPase signaling - Where are we now? [Internet]. Vol. 123, Journal of Cell Science. The Company of Biologists Ltd; 2010 [cited 2021 Feb 24]. p.

1841–50. Available from: https://jcs.biologists.org/content/123/11/1841

11. Nalbant P, Dehmelt L. Exploratory cell dynamics: A sense of touch for cells? Biol Chem [Internet]. 2018 Jul 26 [cited 2022 Apr 25];399(8):809–19. Available from: https://www.degruyter.com/document/doi/10.1515/hsz-2017-0341/html?lang=en

12. Graessl M, Koch J, Calderon A, Kamps D, Banerjee S, Mazel T, et al. An excitable Rho GTPase signaling network generates dynamic subcellular contraction patterns. J Cell Biol [Internet]. 2017 Dec 4 [cited 2021 Feb 24];216(12):4271–85. Available from: https://doi.org/10.1083/jcb.201706052

13. Müller PM, Rademacher J, Bagshaw RD, Wortmann C, Barth C, van Unen J, et al. Systems analysis of RhoGEF and RhoGAP regulatory proteins reveals spatially organized RAC1 signalling from integrin adhesions. Nat Cell Biol [Internet]. 2020;22(4):498–511. Available from: http://dx.doi.org/10.1038/s41556-020-0488-x

14. Thé M, Racine V, Piel M, Pépin A, Dimitrov A, Chen Y, et al. Anisotropy of cell adhesive microenvironment governs cell internal organization and orientation of polarity. Proc Natl Acad Sci U S A. 2006;103(52):19771–6.

15. Théry M. Micropatterning as a tool to decipher cell morphogenesis and functions. J Cell Sci [Internet]. 2010 Dec 15 [cited 2022 Mar 6];123(24):4201–13. Available from: https://journals.biologists.com/jcs/article/123/24/4201/31394/Micropatterning-as-a-tool-to-decipher-cell

16. Friedl P, Gilmour D. Collective cell migration in morphogenesis, regeneration and cancer. Nat Rev Mol Cell Biol 2009 107 [Internet]. 2009 Jul [cited 2022 Mar 6];10(7):445–57. Available from: https://www.nature.com/articles/nrm2720

17. Ladoux B, Mège R-M, Trepat X. Front–Rear Polarization by Mechanical Cues: From Single Cells to Tissues Front–Rear Polarity in Single Cells and Cell Ensembles. Trends Cell Biol [Internet]. 2016;26(6):420–33. Available from: https://ac.els-cdn.com/S0962892416000143/1-s2.0-S0962892416000143-main.pdf?_tid=3cc4ff5c-adbb-11e7-bd47-00000aacb35e&acdnat=1507640716_05c574a654f5c2fb60b26f87f838477e

18. De Oliveira S, Rosowski EE, Huttenlocher A. Neutrophil migration in infection and wound repair: going forward in reverse. Nat Rev Immunol 2016 166 [Internet]. 2016 May 27 [cited 2021 Dec 20];16(6):378–91. Available from: https://www.nature.com/articles/nri.2016.49

19. Shellard A, Mayor R. Collective durotaxis along a self-generated stiffness gradient in vivo. Nat 2021 6007890 [Internet]. 2021 Dec 8 [cited 2022 Feb 4];600(7890):690–4. Available from: https://www.nature.com/articles/s41586-021-04210-x

20. Sheng Wong B, Mistriotis P, Konstantopoulos K, Wong BS, Mistriotis P, Konstantopoulos K. Exposing Cell-Itary Confinement: Understanding the Mechanisms of Confined Single Cell Migration. Adv Exp Med Biol [Internet]. 2018 [cited 2022 Mar 6];1092:139–57. Available from: https://link.springer.com/chapter/10.1007/978-3-319-95294-9_8

21. Mayor R, Etienne-Manneville S. The front and rear of collective cell migration. Nat Rev Mol Cell Biol 2016 172 [Internet]. 2016 Jan 4 [cited 2021 Jul 8];17(2):97–109. Available from: https://www.nature.com/articles/nrm.2015.14

22. Hayer A, Shao L, Chung M, Joubert LM, Yang HW, Tsai FC, et al. Engulfed cadherin fingers are polarized junctional structures between collectively migrating endothelial cells. Nat Cell Biol [Internet]. 2016 Dec 1 [cited 2021 Mar 2];18(12):1311–23. Available from: https://www.nature.com/articles/ncb3438

23. Ozawa M, Hiver S, Yamamoto T, Shibata T, Upadhyayula S, Mimori-Kiyosue Y, et al. Adherens junction regulates cryptic lamellipodia formation for epithelial cell migration. J Cell Biol. 2020 Oct 5;219(10).

24. Charras G, Sahai E. Physical influences of the extracellular environment on cell migration. Nat Rev Mol Cell Biol [Internet]. 2014 Dec 11 [cited 2021 May 25];15(12):813–24. Available from: www.nature.com/reviews/molcellbio

25. Rappel WJ, Edelstein-Keshet L. Mechanisms of Cell Polarization. Curr Opin Syst Biol [Internet]. 2017 Jun 1 [cited 2022 Apr 10];3:43. Available from: /pmc/articles/PMC5640326/

26. Tozluoğlu M, Tournier AL, Jenkins RP, Hooper S, Bates PA, Sahai E. Matrix geometry determines optimal cancer cell migration strategy and modulates response to interventions. Nat Cell Biol 2013 157 [Internet]. 2013 Jun 23 [cited 2022 Apr 10];15(7):751–62. Available from: https://www.nature.com/articles/ncb2775

27. Gordon E, Schimmel L, Frye M. The Importance of Mechanical Forces for in vitro Endothelial Cell Biology [Internet]. Vol. 11, Frontiers in Physiology. Frontiers Media S.A.; 2020 [cited 2021 May 6]. p. 684. Available from: www.frontiersin.org

28. Gómez-Moutón C, Mañes S. Establishment and Maintenance of Cell Polarity During Leukocyte Chemotaxis. Cell Adh Migr [Internet]. 2007 [cited 2022 Apr 16];1(2):69. Available from: /pmc/articles/PMC2633974/

29. Bodor DL, Pönisch W, Endres RG, Paluch EK. Of Cell Shapes and Motion: The Physical Basis of Animal Cell Migration. Dev Cell. 2020 Mar 9;52(5):550–62.

30. Ridley AJ. Life at the leading edge. Cell. 2011;145(7):1012–22.

31. Etienne-Manneville S. Polarity proteins in migration and invasion. Oncogene. 2008;27(55):6970–80.

32. Campanale JP, Sun TY, Montell DJ. Development and dynamics of cell polarity at a glance. J Cell Sci [Internet]. 2017 Apr 1 [cited 2022 Apr 15];130(7):1201. Available from: /pmc/articles/PMC5399778/

33. Yam PT, Wilson CA, Ji L, Hebert B, Barnhart EL, Dye NA, et al. Actin-myosin network reorganization breaks symmetry at the cell rear to spontaneously initiate polarized cell motility. J Cell Biol. 2007;178(7):1207–21.

34. Devreotes P, Horwitz AR. Signaling Networks that Regulate Cell Migration. Cold Spring Harb Perspect Biol [Internet]. 2015 Aug 1 [cited 2022 Mar 6];7(8). Available from: /pmc/articles/PMC4526752/

35. Etienne-Manneville S, Hall A. Rho GTPases in cell biology. Nat 2002 4206916 [Internet]. 2002 Dec 12 [cited 2022 Jan 9];420(6916):629–35. Available from: https://www.nature.com/articles/nature01148

36. Ridley AJ. Rho GTPase signalling in cell migration. Curr Opin Cell Biol. 2015 Oct 1;36:103–12.

37. Hodge RG, Ridley AJ. Regulating Rho GTPases and their regulators. Nat Rev Mol Cell Biol 2016 178 [Internet]. 2016 Jun 15 [cited 2022 Apr 25];17(8):496–510. Available from: https://www.nature.com/articles/nrm.2016.67

38. Ridley AJ. Rho GTPases and cell migration. J Cell Sci [Internet]. 2001 Aug 1 [cited 2022 Mar 6];114(15):2713–22. Available from: https://journals.biologists.com/jcs/article/114/15/2713/35266/Rho-GTPases-and-cell-migration

39. Kühn S, Erdmann C, Kage F, Block J, Schwenkmezger L, Steffen A, et al. The structure of FMNL2–Cdc42 yields insights into the mechanism of lamellipodia and filopodia formation. Nat Commun 2015 61 [Internet]. 2015 May 12 [cited 2022 May 27];6(1):1–14. Available from: https://www.nature.com/articles/ncomms8088

40. Fortin Ensign SP, Mathews IT, Symons MH, Berens ME, Tran NL. Implications of Rho GTPase signaling in glioma cell invasion and tumor progression. Front Oncol. 2013;3 OCT:241.

41. Dipankar P, Kumar P, Dash SP, Sarangi PP. Functional and Therapeutic Relevance of Rho GTPases in Innate Immune Cell Migration and Function during Inflammation: An In Silico Perspective. Mediators Inflamm [Internet]. 2021 [cited 2022 May 22];2021. Available from: /pmc/articles/PMC7896857/

42. Bos JL, Rehmann H, Wittinghofer A. GEFs and GAPs: Critical Elements in the Control of Small G Proteins. Cell. 2007 Jun 1;129(5):865–77.

43. Kreider-Letterman G, Carr NM, Garcia-Mata R. Fixing the GAP: The role of RhoGAPs in cancer. Eur J Cell Biol. 2022 Apr 1;101(2):151209.

44. DerMardirossian C, Bokoch GM. GDIs: central regulatory molecules in Rho GTPase activation. Trends Cell Biol. 2005 Jul 1;15(7):356–63.

45. Guilluy C, Garcia-Mata R, Burridge K. Rho protein crosstalk: Another social network? Trends Cell Biol. 2011 Dec;21(12):718–26.

46. Garcia-Mata R, Boulter E, Burridge K. The "invisible hand": regulation of RHO GTPases by RHOGDIs. Nat Rev Mol Cell Biol 2011 128 [Internet]. 2011 Jul 22 [cited 2022 May 22];12(8):493–504. Available from: https://www.nature.com/articles/nrm3153

47. Liu M, Bi F, Zhou X, Zheng Y. Rho GTPase regulation by miRNAs and covalent modifications. Trends Cell Biol [Internet]. 2012 Jul [cited 2022 May 15];22(7):365. Available from: /pmc/articles/PMC3383930/

48. Croft DR, Olson MF. Transcriptional regulation of Rho GTPase signaling. Transcription [Internet]. 2011 [cited 2022 May 15];2(5):211. Available from: /pmc/articles/PMC3265777/

49. Algar WR, Hildebrandt N, Vogel SS, Medintz IL. FRET as a biomolecular research tool — understanding its potential while avoiding pitfalls. Nat Methods 2019 169 [Internet]. 2019 Aug 30 [cited 2022 Apr 25];16(9):815–29. Available from: https://www.nature.com/articles/s41592-019-0530-8

50. Donnelly SK, Bravo-Cordero JJ, Hodgson L. Rho GTPase isoforms in cell motility: Don't fret, we have FRET. Cell Adh Migr [Internet]. 2014 Nov 1 [cited 2022 Apr 30];8(6):526. Available from: /pmc/articles/PMC4594258/

51. Fluorescence Resonance Energy Transfer (FRET) Microscopy - Introductory Concepts | Olympus LS.

52. Basics of FRET Microscopy | Nikon's MicroscopyU.

53. Pertz O, Hahn KM. Designing biosensors for Rho family proteins — deciphering the dynamics of Rho family GTPase activation in living cells. J Cell Sci [Internet]. 2004 Mar 15 [cited 2022 May 10];117(8):1313–8. Available from: https://journals.biologists.com/jcs/article/117/8/1313/28263/Designing-biosensors-for-Rho-family-proteins

54. Mahlandt EK, Arts JJG, van der Meer WJ, van der Linden FH, Tol S, van Buul JD, et al. Visualizing endogenous Rho activity with an improved localization-based, genetically encoded biosensor. J Cell Sci [Internet]. 2021 Sep 1 [cited 2022 May 10];134(17). Available from:

https://journals.biologists.com/jcs/article/134/17/jcs258823/272101/Visualizing-endogenous-Rho-activity-with-an

55. Dominik Fritz R, Pertz O, Debant A, Hodgson L. The dynamics of spatio-temporal Rho GTPase signaling: formation of signaling patterns. F1000Research 2016 5749 [Internet]. 2016 Apr 26 [cited 2022 May 7];5:749. Available from: https://f1000research.com/articles/5-749

56. Martin K, Reimann A, Fritz RD, Ryu H, Jeon NL, Pertz O. Spatio-temporal co-ordination of RhoA, Rac1 and Cdc42 activation during prototypical edge protrusion and retraction dynamics. Sci Reports 2016 61 [Internet]. 2016 Feb 25 [cited 2022 May 7];6(1):1–14. Available from: https://www.nature.com/articles/srep21901

57. Marston DJ, Vilela M, Huh J, Ren J, Azoitei ML, Glekas G, et al. Multiplexed GTPase and GEF biosensor imaging enables network connectivity analysis. Nat Chem Biol 2020 168 [Internet]. 2020 May 18 [cited 2022 Apr 25];16(8):826–33. Available from: https://www.nature.com/articles/s41589-020-0542-9

58. Bolado-Carrancio A, Rukhlenko OS, Nikonova E, Tsyganov MA, Wheeler A, Garcia-Munoz A, et al. Periodic propagating waves coordinate RhoGTPase network dynamics at the leading and trailing edges during cell migration. [cited 2022 Apr 25]; Available from: https://doi.org/10.7554/eLife.58165

59. De Pascalis C, Etienne-Manneville S. Single and collective cell migration: The mechanics of adhesions. Mol Biol Cell [Internet]. 2017 Jul 7 [cited 2022 May 24];28(14):1833–46. Available from: https://www.molbiolcell.org/doi/full/10.1091/mbc.e17-03-0134

60. Kanchanawong P, Shtengel G, Pasapera AM, Ramko EB, Davidson MW, Hess HF, et al. Nanoscale architecture of integrin-based cell adhesions. Nat 2010 4687323 [Internet]. 2010 Nov 24 [cited 2022 May 24];468(7323):580–4. Available from: https://www.nature.com/articles/nature09621

61. Geiger B, Spatz JP, Bershadsky AD. Environmental sensing through focal adhesions. Nat Rev Mol Cell Biol 2009 101 [Internet]. 2009 Jan [cited 2022 May 24];10(1):21–33. Available from: https://www.nature.com/articles/nrm2593

62. Kechagia JZ, Ivaska J, Roca-Cusachs P. Integrins as biomechanical sensors of the microenvironment. Nat Rev Mol Cell Biol 2019 208 [Internet]. 2019 Jun 10 [cited 2021 Oct 26];20(8):457–73. Available from: https://www.nature.com/articles/s41580-019-0134-2

63. Palecek SP, Loftus JC, Ginsberg MH, Lauffenburger DA, Horwitz AF, Deshpande PP, et al. Integrin – ligand binding properties govern cell migration speed through cell – substratum adhesiveness Total synthesis of the potential anticancer vaccine KH-1 adenocarcinoma antigen Integrin – ligand binding properties govern cell migration speed throug. 1997;388(July).

64. Ladoux B, Mège RM. Mechanobiology of collective cell behaviours [Internet]. Vol. 18, Nature Reviews Molecular Cell Biology. Nature Publishing Group; 2017. p. 743–57. Available from: http://dx.doi.org/10.1038/nrm.2017.98

65. Bazellières E, Conte V, Elosegui-Artola A, Serra-Picamal X, Bintanel-Morcillo M, Roca-Cusachs P, et al. Control of cell-cell forces and collective cell dynamics by the intercellular adhesome. Nat Cell Biol [Internet]. 2015 Apr 30 [cited 2021 Jun 14];17(4):409–20. Available from: https://www.nature.com/articles/ncb3135

66. C Harris TJ, Tepass U. Adhesive forces prevent animal tissues from dissociating into. 2010 [cited 2022 Jun 20]; Available from: www.nature.com/reviews/molcellbio

67. Hahn C, Schwartz MA. Mechanotransduction in vascular physiology and atherogenesis. 2009;10(jAnuAry).

68. Wettschureck N, Strilic B, Offermanns S. Passing the vascular barrier: Endothelial signaling processes controlling extravasation. Physiol Rev [Internet]. 2019 Jul 1 [cited 2022 Jun 21];99(3):1467–525. Available from: https://journals.physiology.org/doi/10.1152/physrev.00037.2018

69. D'Arcangelo E, McGuigan AP. Micropatterning strategies to engineer controlled cell and tissue architecture in vitro. Biotechniques. 2015;58(1):13–23.

70. Théry M, Pépin A, Dressaire E, Chen Y, Bornens M. Cell distribution of stress fibres in response to the geometry of the adhesive environment. Cell Motil Cytoskeleton.

2006;63(6):341–55.

71. Alom S, Ab R, Chen CS. Microcontact printing: A tool to pattern. 1999 [cited 2022 May 2]; Available from: www.rsc.org/softmatter

72. Jiang X, Bruzewicz DA, Wong AP, Piel M, Whitesides GM. Directing cell migration with asymmetric micropatterns. Proc Natl Acad Sci U S A [Internet]. 2005 Jan 25 [cited 2022 May 7];102(4):975–8. Available from: www.pnas.orgcgidoi10.1073pnas.0408954102

73. Lo Vecchio S, Thiagarajan R, Caballero D, Vigon V, Navoret L, Voituriez R, et al. Collective Dynamics of Focal Adhesions Regulate Direction of Cell Motion. Cell Syst. 2020;10(6):535-542.e4.

74. Jain S, Cachoux VML, Narayana GHNS, de Beco S, D'Alessandro J, Cellerin V, et al. The role of single-cell mechanical behaviour and polarity in driving collective cell migration. Nat Phys [Internet]. 2020 Jul 1 [cited 2021 Mar 2];16(7):802–9. Available from: https://doi.org/10.1038/s41567-020-0875-z

75. Vishwakarma M, Di Russo J, Probst D, Schwarz US, Das T, Spatz JP. Mechanical interactions among followers determine the emergence of leaders in migrating epithelial cell collectives. Nat Commun 2018 91 [Internet]. 2018 Aug 27 [cited 2022 May 9];9(1):1–12. Available from: https://www.nature.com/articles/s41467-018-05927-6

76. Wu PH, Gilkes DM, Phillip JM, Narkar A, Cheng TWT, Marchand J, et al. Single-cell morphology encodes metastatic potential. Sci Adv [Internet]. 2020 Jan 22 [cited 2022 May 23];6(4). Available from: https://www.science.org/doi/full/10.1126/sciadv.aaw6938

77. Andrews TGR, Pönisch W, Paluch EK, Steventon BJ, Benito-Gutierrez E. Single-cell morphometrics reveals ancestral principles of notochord development. Dev [Internet]. 2021 Aug 1 [cited 2022 May 24];148(18). Available from: https://journals.biologists.com/dev/article/148/16/dev199430/271871/Single-cell-morphometrics-reveals-ancestral

78. Keren K, Pincus Z, Allen GM, Barnhart EL, Marriott G, Mogilner A, et al. Mechanism of shape determination in motile cells. Nat 2008 4537194 [Internet]. 2008 May 22 [cited 2022 May 22];453(7194):475–80. Available from:

https://www.nature.com/articles/nature06952

79. Tweedy L, Meier B, Stephan J, Heinrich D, Endres RG. Distinct cell shapes determine accurate chemotaxis. Sci Reports 2013 31 [Internet]. 2013 Sep 6 [cited 2022 May 23];3(1):1–7. Available from: https://www.nature.com/articles/srep02606

80. Reinhard NR, Van Helden SF, Anthony EC, Yin T, Wu YI, Goedhart J, et al. Spatiotemporal analysis of RhoA/B/C activation in primary human endothelial cells. Sci Reports 2016 61 [Internet]. 2016 May 5 [cited 2022 Mar 6];6(1):1–16. Available from: https://www.nature.com/articles/srep25502

81. Itoh RE, Kurokawa K, Ohba Y, Yoshizaki H, Mochizuki N, Matsuda M. Activation of Rac and Cdc42 Video Imaged by Fluorescent Resonance Energy Transfer-Based Single-Molecule Probes in the Membrane of Living Cells. Mol Cell Biol. 2002;22(18):6582–91.

82. Phillip JM, Han K-S, Chen W-C, Wirtz D, Wu P-H. A robust unsupervised machine-learning method to quantify the morphological heterogeneity of cells and nuclei. Nat Protoc [Internet]. Available from: https://doi.org/10.1038/s41596-020-00432-x

83. Ho J, Tumkaya T, Aryal S, Choi H, Claridge-Chang A. Moving beyond P values: data analysis with estimation graphics. Nat Methods 2019 167 [Internet]. 2019 Jun 19 [cited 2022 Jun 23];16(7):565–6. Available from: https://www.nature.com/articles/s41592-019-0470-3

84. Vedula SRK, Leong MC, Lai TL, Hersen P, Kabla AJ, Lim CT, et al. Emerging modes of collective cell migration induced by geometrical constraints. Proc Natl Acad Sci U S A. 2012 Aug 7;109(32):12974–9.

85. Lamouille S, Xu J, Derynck R. Molecular mechanisms of epithelial–mesenchymal transition. Nat Rev Mol Cell Biol [Internet]. 2014 Mar [cited 2022 Aug 9];15(3):178. Available from: /pmc/articles/PMC4240281/

86. Ciszewski WM, Sobierajska K, Wawro ME, Klopocka W, Chefczyńska N, Muzyczuk A, et al. The ILK-MMP9-MRTF axis is crucial for EndMT differentiation of endothelial cells in a tumor microenvironment. Biochim Biophys Acta - Mol Cell Res. 2017 Dec 1;1864(12):2283–96.

87. Aoki K, Maeda F, Nagasako T, Mochizuki Y, Uchida S, Ikenouchi J. A RhoA and Rnd3 cycle regulates actin reassembly during membrane blebbing. Proc Natl Acad Sci [Internet]. 2016 Mar 29 [cited 2021 Oct 6];113(13):E1863–71. Available from: https://www.pnas.org/content/113/13/E1863

88. Jiao M, Wu D, Wei Q. Myosin II–interacting guanine nucleotide exchange factor promotes bleb retraction via stimulating cortex reassembly at the bleb membrane. Blanchoin L, editor. Mol Biol Cell [Internet]. 2018 Mar 1 [cited 2021 Feb 24];29(5):643–56. Available from: https://www.molbiolcell.org/doi/10.1091/mbc.E17-10-0579